Fall 2011

Combustion dynamics of individual reactive material particles

Carlo Francisco Badiola
New Jersey Institute of Technology

Copyright Warning & Restrictions

The copyright law of the United States (Title 17, United States Code) governs the making of photocopies or other reproductions of copyrighted material.

Under certain conditions specified in the law, libraries and archives are authorized to furnish a photocopy or other reproduction. One of these specified conditions is that the photocopy or reproduction is not to be "used for any purpose other than private study, scholarship, or research." If a, user makes a request for, or later uses, a photocopy or reproduction for purposes in excess of "fair use" that user may be liable for copyright infringement,

This institution reserves the right to refuse to accept a copying order if, in its judgment, fulfillment of the order would involve violation of copyright law.

Please Note: The author retains the copyright while the New Jersey Institute of Technology reserves the right to distribute this thesis or dissertation

Printing note: If you do not wish to print this page, then select "Pages from: first page # to: last page #" on the print dialog screen

ABSTRACT

COMBUSTION DYNAMICS OF INDIVIDUAL REACTIVE MATERIAL PARTICLES

by
Carlo Francisco Badiola

Metallic reactive powders are widely used as solid fuels, pyrotechnic materials, and components of enhanced blast explosives. Metals are attractive because of their high combustion enthalpies and temperatures. Quantitative descriptions of the combustion processes and mechanisms for both pure metal and composite particles are also desired for their proper implementation in specific applications. Among reactive metals, Al is used most widely and its combustion has been studied extensively. A recently developed experimental setup using laser-ignited metal powders enabled one to record optical signatures for time-resolved combustion instances for 2-25 μm diameter aluminum particles burning in different atmospheres. Individual particle diameters are interpreted and emission signatures are correlated to determine the burn times. The current setup has been expanded to include three-color optical pyrometry and tracing characteristic molecular emission. Results for Al and novel Al-based composite materials burning in different oxidizing environments will be discussed.

COMBUSTION DYNAMICS OF INDIVIDUAL REACTIVE MATERIAL PARTICLES

by
Carlo Francisco Badiola

A Thesis
Submitted to the Faculty of
New Jersey Institute of Technology
in Partial Fulfillment of the Requirements for the Degree of
Master of Science in Chemical Engineering

Department of Chemical, Biological, and Pharmaceutical Engineering

January 2012

APPROVAL PAGE

COMBUSTION DYNAMICS OF INDIVIDUAL REACTIVE MATERIAL PARTICLES

Carlo Francisco Badiola

Dr. Edward L. Dreizin, Thesis Advisor — Date
Professor of Chemical, Biological, and Pharmaceutical Engineering, NJIT

Dr. Robert B. Barat, Committee Member — Date
Professor of Chemical, Biological, and Pharmaceutical Engineering, NJIT

Dr. Mirko Schoenitz, Committee Member — Date
Associate Research Professor of Chemical, Biological, and Pharmaceutical Engineering, NJIT

BIOGRAPHICAL SKETCH

Author: Carlo Francisco Badiola

Degree: Master of Science

Date: January 2012

Undergraduate and Graduate Education:

- Master of Science in Chemical Engineering,
  New Jersey Institute of Technology, Newark, NJ, 2012

- Bachelor of Science in Chemical Engineering,
  New Jersey Institute of Technology, Newark, NJ, 2010

- Bachelor of Science in Mechanical Engineering,
  New Jersey Institute of Technology, Newark, NJ, 2010

Major: Chemical Engineering

Presentations and Publications:

Badiola, C., Gill, R. J., and Dreizin, E. L. "Combustion characteristics of micron-sized aluminum particles in oxygenated environments," *Combustion and Flame* Vol. 158, No. 10, 2011, pp. 2064-2070.

Gill, R. J., Badiola, C., and Dreizin, E. L. "Combustion times and emission profiles of micron-sized aluminum particles burning in different environments," *Combustion and Flame* Vol. 157, No. 11, 2010, pp. 2015-2023.

Badiola, C., Schoenitz, M., Zhu, X., and Dreizin, E. L. "Nanocomposite thermite powders prepared by cryomilling," *Journal of Alloys and Compounds* Vol. 488, No. 1, 2009, pp. 386-391.

Badiola, C., Zhang, S., Aly, Y., and Dreizin, E.L., "Combustion rates and temperatures of reactive material particles," US National Technical Meeting of the Combustion Institute, Atlanta, GA, 2011.

Badiola, C., Zhang, S., Gill, R., and Dreizin, E.L., "Combustion rates and temperatures of reactive materials particles," 49th AIAA Aerospace Sciences Meeting, Orlando, FL, 2011.

Badiola, C., Gill, R., and Dreizin, E.L., "Combustion characteristics of micron-sized metal and metal-composite particles in different environments," 10th AIChE Annual Meeting, Salt Lake City, UT, 2010.

Badiola, C., Schoenitz, M., and Dreizin, E.L., "Mechanically alloyed Al-Ti powders prepared by mechanical milling at cryogenic temperatures," 45th AIAA/ASME/SAE/ASEE Joint Propulsion Conference and Exhibit, Denver, CO, 2009.

Badiola, C., Schoenitz, M., Zhu, X., and Dreizin, E.L., "Aluminum rich Al-CuO nanocomposite materials prepared by arrested reactive milling at cryogenic and room temperatures," 47th AIAA Aerospace Science Meeting, Orlando, FL, 2009.

Badiola, C., Schoenitz, M., Zhu, X., and Dreizin, E.L., "Synthesis and characterization of aluminum-rich nanocomposite powders at cryogenic temperatures," AIChE Annual Meeting, Philadelphia, PA, 2008.

Badiola, C., Schoenitz, M., and Dreizin, E.L., "Synthesis of aluminum-rich nanocomposite powders at cryogenic temperatures," 44th AIAA/ASME/SAE/ASEE Joint Propulsion Conference and Exhibit, Hartford, CT, 2008.

"*To laugh often and much; to win the respect of intelligent people and the affection of children; to earn the appreciation of honest critics and endure the betrayal of false friends; to appreciate beauty; to find the best in others; to leave the world a bit better, whether by a healthy child, a garden patch or a redeemed social condition; to know even one life breathed easier because you have lived. <u>This</u> is to have succeeded.*"

- Ralph Waldo Emerson

To my family, Edgar, Grace, Katrina, and Patricia - for all your unceasing support and limitless love

To Jan, from the first day of this journey to the last

ACKNOWLEDGMENT

I would like to express my deepest appreciation and gratitude to Dr. Edward Dreizin for serving as my undergraduate and graduate research advisor. I will always be indebted to Dr. Dreizin for giving me these opportunities and all of the mentoring, direction, support, and resources he provided which made this work possible. Special thanks are given to Dr. Robert Barat and Dr. Mirko Schoenitz for actively participating in my committee and providing valuable feedback.

I would like to thank the Defense Threat Reduction Agency (DTRA) for supporting this work at NJIT. The interest and encouragement from Drs. Sue Peiris and William Wilson of DTRA are gratefully acknowledged.

Thanks to staff at the Energetic Materials Laboratory. I'm especially grateful to Dr. Robert Gill for giving me technical insight and mentoring me throughout my work.

TABLE OF CONTENTS

TABLE OF CONTENTS
(Continued)

LIST OF TABLES

LIST OF FIGURES

LIST OF FIGURES
(Continued)

LIST OF FIGURES
(Continued)

Figure **Page**

LIST OF FIGURES
(Continued)

Figure **Page**

CHAPTER 1

INTRODUCTION

Aluminum powder is a widely used and studied fuel additive for solid propellants, explosives, and pyrotechnics [1-3]; it is also a benchmark for development of many advanced reactive materials. Furthermore, aluminum serves as the main component of multiple novel reactive compositions [3-5]. Developers of the new materials aim to achieve reduced particle ignition temperatures, greater reaction rates [4, 7] or specific desired reaction products [8-10]. Much interest is focused on understanding the combustion dynamics of new materials, but detailed experimental studies are limited. Even for pure aluminum, current reaction models are oversimplified and assume steady reaction rates [11, 12], despite substantial experimental evidence of multiple stages in Al particle combustion [13]. Currently, efforts aimed to design and synthesize new compositions outpace the development of laboratory methods needed to characterize and understand their combustion behavior. The characterization efforts are particularly challenging considering that typical particle sizes of powders of interest are in the range of 1-50 μm. A new experimental setup developed in references [14-16] uses laser ignition to study combustion of single, micron-sized metal particles. In this effort, the experimental setup is modified to handle ESD-ignition sensitive nanocomposite materials.

CHAPTER 2

COMBUSTION TIMES AND EMISSION PROFILES OF MICRON-SIZED ALUMINUM PARTICLES BURNING IN DIFFERENT ENVIRONMENTS

Optical signatures and combustion times for micron-sized aluminum particles are measured in oxidizing environments including nitrogen mixtures with oxygen, carbon dioxide, and water. Particles in a room temperature oxidizing gas stream are fed into a CO_2 laser beam where they are ignited. Prior to entering the CO_2 laser beam, each particle crosses a second, low energy laser beam and produces a scattered light signal used to determine the particle size in real time. The correlation between the measured particle sizes and their burn times produces an experimental trend that is compared to various correlations reported in the literature. In addition to the burn time measurements, detailed optical signatures are recorded for micron-sized aluminum particles burning in different environments. For aluminum burning in water vapor, the optical signature of the particle is substantially weaker than in other environments, possibly indicating a primarily surface oxidation. It is shown that semi-empirical and widely used $\tau_b \sim D^n$ expressions for the particle burn time, τ_b, as a function of its diameter, D, are inaccurate for the conditions that are different from those used to establish respective trends initially. It is observed that the effect of oxygen concentration on combustion time of micron-sized aluminum particles is weak when oxygen concentrations exceed 21%. Combustion times increase substantially for lower oxygen concentrations. Aluminum particle combustion times are substantially longer than predicted for experiments with water and carbon dioxide oxidizers. For all environments, the observed effect of particle size is relatively weak and the exponents in the descriptive D^n relations appropriate for the current

experiments vary approximately from 0.3 to 1. The exponent close to 0.3 adequately describes current results for those oxidizing environments for which heterogeneous reactions appear to dominate.

2.1 Introduction

Aluminum is an important energetic component of many solid propellants, explosives, and pyrotechnic formulations [17-20]. One critical parameter of aluminum combustion, universally important for all applications, is the particle burn time, τ_b, as a function of the particle diameter, D. For practical purposes the burn time is commonly expressed as a power law $\tau_b \sim D^n$, with the exponent n and pre-exponent factor depending on the oxidizing environment, temperature, and pressure, e.g., [6, 21-23]. Various D^n type trends were reported by different authors based on a diverse set of experiments. Generally, laboratory experiments in well-characterized environments reported in the literature can be broadly divided into two groups: experiments using individual metal particles, e.g., [13, 24-28], and experiments employing aerosolized powders or clouds, e.g., [22, 29-33]. For individual particles, the measurements of combustion times are often direct, while indirect methods and data analyses are used to extract the information on particle burn times or burn rates from the cloud combustion experiments. It is also worth noting that single metal particle combustion experiments in general, and direct measurements of combustion times for individual aluminum droplets in particular, were restricted to relatively large particles, with sizes 50 μm or greater. However, most practical applications deal with finer aluminum powders with particle sizes on the order of, or finer than, 20 μm. It is also interesting that in many experimental configurations, aluminum particles burn in combustion products of hydrocarbon fuels. In such cases, the oxidizers

are mixtures of CO_2, H_2O, and O_2 in various proportions. While this situation imitates some practical applications, the specific oxidizer mixtures produced in laboratory burners and in practical energetic formulations differ from one another substantially. Laboratory experiments with mixed oxidizers are also not particularly useful for extracting the information about efficiency of individual oxidizing species, which is required to model the practical configurations. The information on aluminum combustion in CO_2 and H_2O is very limited [24, 34, 35], with most data coming from experiments in mixed oxidizers, where the effects of different oxidizers are somewhat difficult to uncouple.

Considering the limitations of the available data on aluminum combustion, the goal of the current work was to directly measure optical signatures and burn times of individual, micron-sized aluminum particles. The focus of these experiments was to establish a direct correlation between particle diameters and their optical signatures and burn times for particles under 20 μm. The measurements were performed in well-characterized oxidizing environments with individual oxidizers including O_2, CO_2, and H_2O. These measurements are expected to serve as a foundation for development of a mechanistic aluminum combustion model. The model should account for multiple processes occurring in aluminum combustion and is not expected to be limited to a quasi-steady description. At the same time, the model should be relatively simple to enable its implementation in practical calculations. The measurements reported in this paper are expected to help to identify the most important reaction mechanisms and processes to be included into the mechanistic model of aluminum combustion.

2.2 Experimental

2.2.1 Apparatus

The experimental setup used in this study is schematically shown in Figure 2.1. The apparatus, experimental procedure, and data processing steps have been described in detail in a recent publication [16], and only a brief summary is presented here for completeness. Metal powder, comprised of spherical particles, was fed by an electrostatic particle generator [16, 22, 33] so that a narrow, vertically rising particle jet with a low number density is produced. The particles were carried by an oxidizing gas stream. The particle jet crosses two laser beams. Initially, particles intercept a 785-nm laser beam. For each particle, the scattered light intensity is proportional to its area and is used to measure the particle diameter. Two millimeters above the 785 nm laser beam, the particles traverse a focused CO_2 laser beam (~0.3 mm beam waist) in approximately 0.5 ms (i.e., particle velocities ~0.6 m/s). In the CO_2 beam, particles are rapidly heated and ignited. Emission from the incandescent and burning particles was measured to determine the particle burn times. The emission was collected by a wide angle quartz fiber, passed through a 500 nm band-pass filter, detected by a photomultiplier tube, converted to a digital signal, and stored for further analysis.

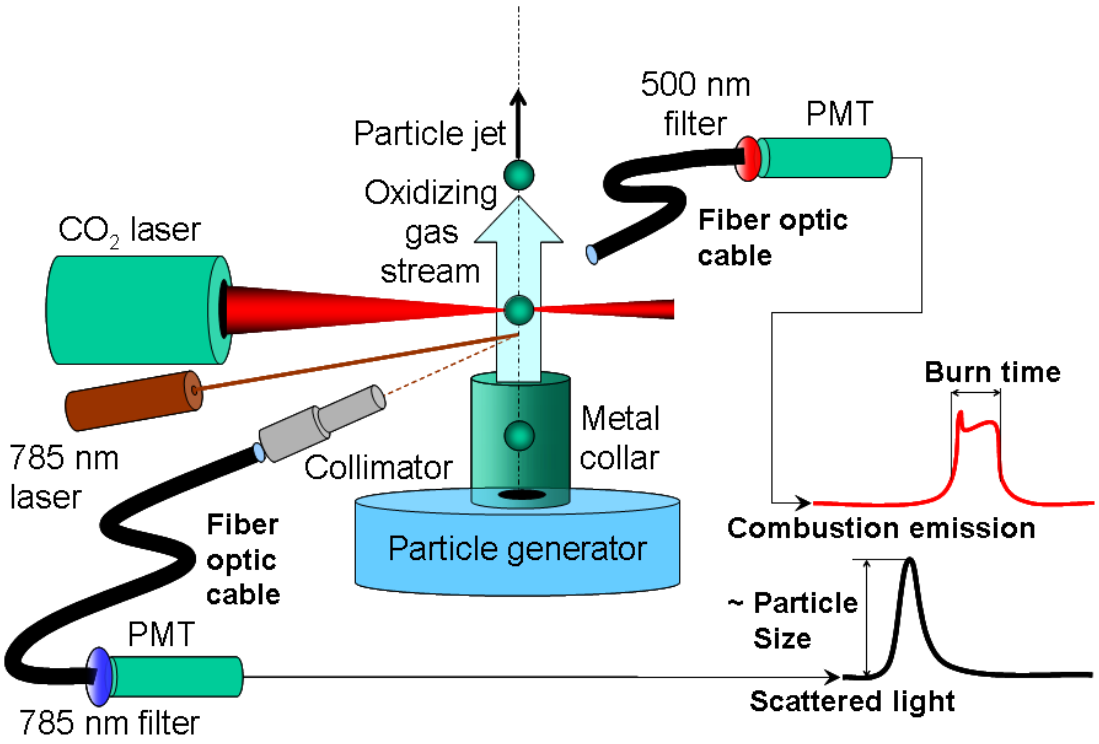

Figure 2.1 Schematic diagram of the experimental setup.

There are three significant modifications to the apparatus previously described in reference [16].

Initially, a set of small inner diameter telescoping tubes, labeled "collimator" in Figure 2.1 were attached to the fiber optic viewing the 785 nm scattered light. The field of view of the detection system was reduced to < 4.5° (full angle) and these tubes eliminated all emission produced by incandescent or burning particles from reaching the scattered light detector.

Second, experiments were performed in various oxidizing environments. The compositions of the oxidizers included mixtures of N_2/O_2, N_2/CO_2, and N_2/H_2O (all at 1 atm). A thin-walled aluminum collar ("metal collar" in Figure 2.1) was added to the particle generator. This restricted outside air from mixing with the oxidizing gas streams. This collar is 8 mm in height and it has an outer diameter of 8.9 mm (inner diameter = 6.4

mm). High purity, dry gases were used for these experiments. Gases were metered through needle valves and flows were measured with mass flow meters (Alicat Scientific; Model M200SCCM-D) to ±1% accuracy. Carbon dioxide and water vapors interfere with the operation of the particle generator; so for experiments with these oxidizers, particles were fed with a pure nitrogen stream, and oxidizers were supplied in a shroud jet [16, 36] not shown in detail in Figure 2.1. Detailed calculations using FLUENT software, for the gas flows in this apparatus, show that the inner and outer gas streams are well-mixed at the height where the particles intercept the CO_2 laser beam. These results are presented in reference [36] where the same experimental configuration was employed to study ignition of aluminum particles in different oxidizers. For oxygen/nitrogen gas mixtures, both the inner gas flow passing through the particle generator and the shroud jet had the same gas composition. Individually metered oxygen and nitrogen gas streams were mixed by passing them through a 3.0 m length of plastic tubing (1/4" OD). To generate water vapor, a calibrated peristaltic pump (Control Company; Model 3384-CC) fed liquid water (3.3 mg/s) into a tube furnace held at a temperature of 200-250°C. The gas transfer lines and a top flange of the particle generator were maintained at 120°C to prevent condensation.

Table 2.1 Gas Environments and Flow Rates for Ignition Experiments

Inner Jet Gas	Outer Jet Gas	Collar ?	Flow Rate, cc/min		Jet Velocity, m/s	
			Inner	Outer	Inner	Outer
Air	Air	No	73.0	158	1.61	0.09
O_2:N_2 1:9	O_2:N_2 1:9	Yes	62.3	141	1.38	0.08
O_2:N_2 2:3	O_2:N_2 2:3	Yes	64.9	125	1.43	0.07
N_2	CO_2	Yes	73.6	165	1.63	0.09
N_2	H_2O:N_2 9:1	Yes	67.5	386	1.49	0.21

Jet velocities are calculated at the exit plane of the respective orifice.

Specific environments used in experiments, gas flows, and calculated flow velocities are shown in Table 2.1. Particle flow velocities along the centerline were measured using square-wave modulated (500Hz; 50% duty cycle) green laser sheet illumination. This yielded particle velocities of about 0.6 m/s at 5 mm above the collar rim (13 mm above the particle generator outlet) and these velocities agree with those estimated from the offset time found when correlating the scattering peaks with the corresponding ignition peaks (see Table 2.1 for details).

Lastly, a 14-bit data acquisition board (DAC, National Instruments, Model PCI-6133) replaced the 12-bit, sequential DAC used in prior work. The new DAC has eight independent D/A converters and a maximum sampling rate of 3.0 MS/s (0.33 μs per sampling event). In the current experiments, the sampling rate was 100 kS/s; or 10 μs per data point; except for the experiments with air, where the sampling rate was increased to 500 kS/s. For each scan, the time during which sequences of pulses of both scattered light and light produced by incandescent particles were continuously collected, was 10 sec. Typically, 50-150 scans were collected for a set of experiments with a selected oxidizing gas mixture.

2.2.2 Materials

Spherically shaped micron sized aluminum particles were used for these experiments (Alfa Aesar, 10-14 μm nominal particle size). Prior to experiments, the powder was dried in a glass vial at 65-85°C under vacuum for more than 2 hours. The vial was quickly capped after opening the vacuum oven and after a cooling period, the sample vial was roll-milled (i.e., milled with an aluminum or Teflon solid rod, 1 cm diameter) for

approximately 20 min. This procedure reduced the number of agglomerated particles, but did not deform the shape of the particles - as confirmed by electron microscopy.

2.2.3 Measurements, Processing, and Interpretations

Prior to each combustion experiment, the particle sizing system was calibrated, as described elsewhere [16]. In these calibrations, particle size distributions measured by a commercial analyzer, LS230 by Beckman-Coulter, was matched with the size distributions determined from the scattered light pulses. Please see reference [16] for details including the particle size distribution for the aluminum powder used in this work.

In each measurement, two separate pulse sequences were acquired simultaneously. In the first sequence, each pulse was produced by the scattered light and its amplitude was proportional to the particle surface area. In the second pulse sequence, each pulse represented an incandescent particle and its duration was equal to the time the particle remained incandescent. The two pulse sequences were correlated with each other to determine the emission duration for each individually sized particle. The details of the correlation procedure are given elsewhere [16]. It is based on matching the two sequences of pulses to each other while determining the “offset time” by which one pulse sequence needs to be shifted in time relative to another one to achieve the match. The offset time was compared to the time a particle travels between the two laser beams, which could be readily found from the average particle velocity and distance between the beams. When the two times were sufficiently close, the experimental results were further processed. A typical experiment includes collecting both pulse sequences during 50 - 150 separate 10 sec. intervals. There were typically 500-2000 scatter signal pulses and 50-100 particle emission pulses in each pair of the collected pulse sequences. After the overlapping peaks

are removed and two sequences are correlated, approximately 20-50 pulses remain in each pulse sequence, representing the number of particles for which both sizes and burn times were determined.

Measurement of the particle size is very straightforward based on the scattered light intensity and calibration [16]. However, interpretation of the pulse durations produced by the incandescent particles is more difficult. To illustrate the problem with this interpretation and how it is addressed, consider a cartoon shown in Figure 2.2. It schematically shows three particles of the same diameter crossing the laser beam at different locations. In one possible scenario, particle 1 is not heated to ignition, particle 2 ignites and starts burning within the laser beam, and particle 3 is heated so that it ignites just when it exits the beam. In such a case, the durations of pulses produced by incandescent particles 1 and 2 would be shorter than the combustion time of interest. For particle 1, duration of emission is simply defined by the time the particle cools off (note that cooling times are very short for particles moving in a room temperature gas. An estimate shows that a 20 μm particle at 2793 K will cool to 933 K in about 5.8 ms, but the particle incandescence at 500 nm (spectral detection window) will drop 3 decades in light intensity (our detection limit) in about 1.5 ms. This is substantially shorter than the observed burn times discussed below). For particle 2, part of its combustion was assisted by the laser beam so that the rate of reaction is accelerated. Thus, only the longest pulse measured for particle 3 represents the burn time of interest. Because this consideration is valid for particles of any dimensions, it is concluded that for each particle size, only the longest measured pulse durations represent the burn times of interest. Considering that majority of particles do not cross the laser beam at the very specific location required to

ignite, but not burn the particle while in the beam, it becomes clear that only a small fraction of the recorded emission pulses carries the useful information about the burn time of interest. In other words, many pulses need to be collected and processed so that the fraction of the pulses reflecting the burn time of interest becomes representative.

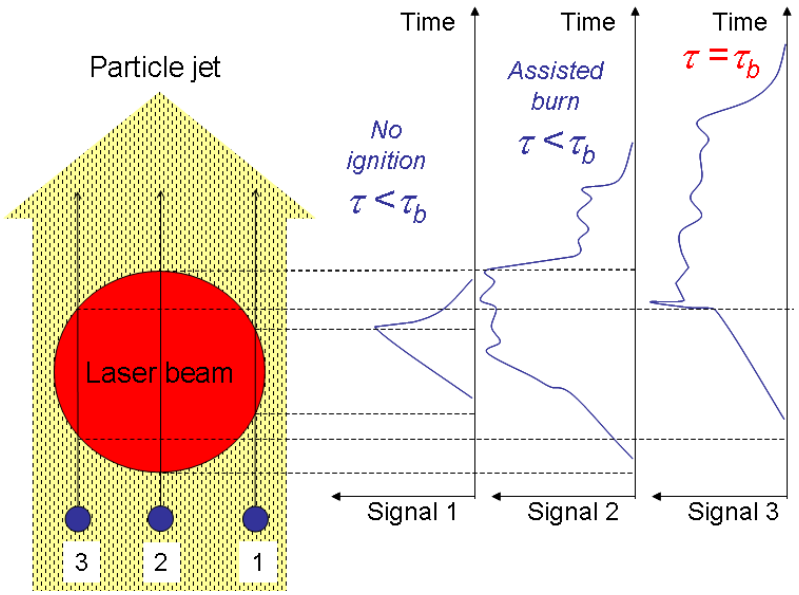

Figure 2.2 Cartoon illustrating formation of pulses of different duration by particles of the same size crossing the laser beam at different locations.

A limitation on the shortest burn time that can be measured reliably is implied by the time a particle crosses the laser beam, so that it may be heated rapidly and remain incandescent while moving within the beam. Roughly, this limitation can be estimated as the ratio of the laser beam waist (~ 300 μm) over the average particle velocity (~ 0.6 m/s) giving a heating time of about 0.5 ms.

2.3 Results

2.3.1 Emission Profiles

The emission intensity profiles from burning Al particles provide information about the processes and reactions occurring during combustion. Characteristic emission profiles for particles burning in different environments are shown in Figures 2.3 – 2.7. The profiles shown are not selected to represent only the longest pulses for each particle size; instead, representative samples of profiles of different durations are shown for all environments.

The profiles measured for Al combustion in oxygen/nitrogen mixtures are collected in Figures 2.3-2.5. The profiles look similar to one another and always begin with a relatively sharp initial peak. A closer examination of the peak fronts shows that for many pulses, the rate of the initial signal rise exhibits a sharp, step-wise increase, possibly indicating particle ignition within the laser beam. For particles burning in 10% O_2, Figure 2.3, the first emission peak is relatively sharp and is followed by a steadily decaying emission signal. The decay is followed by a characteristic oscillatory emission pattern preceding the particle quenching. For particles burning in 21% O_2, the first emission peak becomes wider, while still being followed by a period of nearly steady decay in the emission signal. The oscillatory pattern is less clearly visible, and in many cases the oscillations are reduced to one or two spikes in the emission signal. While the burn time trends are discussed below, it is interesting to note here that the emission pulse durations in general are substantially reduced as the oxygen concentration increases from 10 to 21 %. For particles burning in 40% O_2, the first emission peak is very broad and the oscillatory emission patterns often appear nearly immediately following the peak. The oscillations continue for the entire burn time while the particle extinction is often

preceded by a sharp jump in the emission intensity. No significant reduction in the measured pulse durations is noticed as compared to the pulses obtained in the 21% O_2 environment.

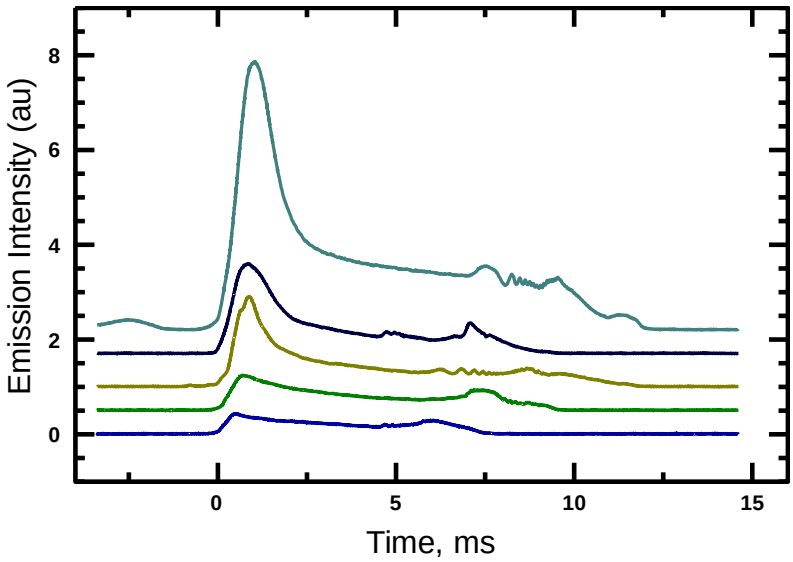

Figure 2.3 Emission profiles for Al particles burning in a 10/90 O_2/N_2 mixture.

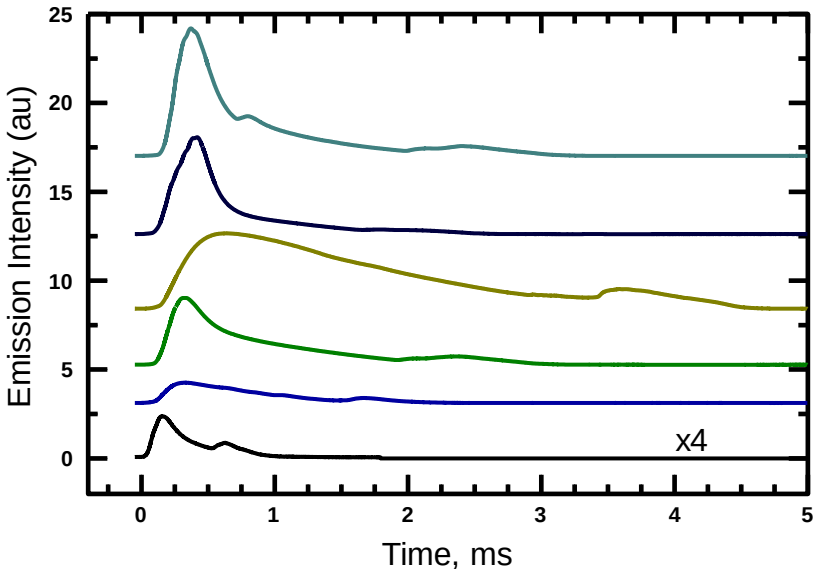

Figure 2.4 Emission profiles for Al particles burning in a 21/79 O_2/N_2 mixture (air).

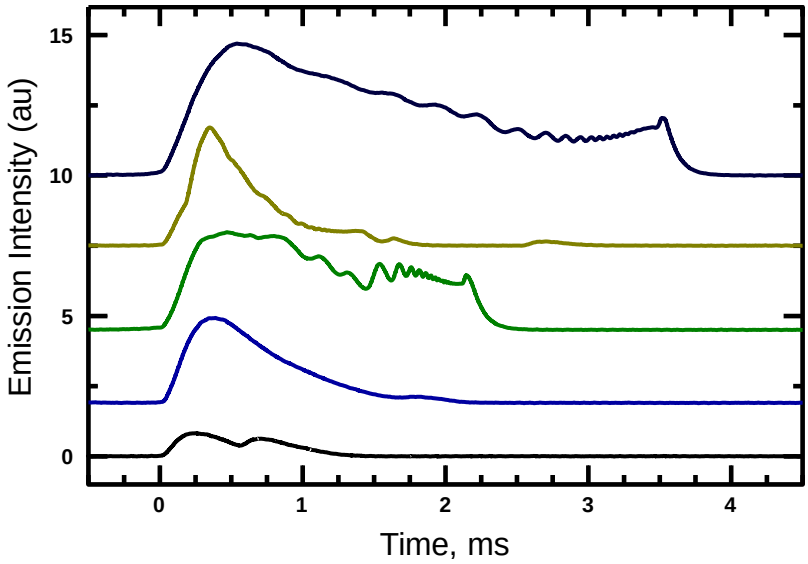

Figure 2.5 Emission profiles for Al particles burning in a 40/60 O_2/N_2 mixture.

The emission profiles for carbon dioxide and water are presented in Figures 2.6 and 2.7, respectively. The carbon dioxide profiles exhibit a broad first peak followed by a long, slow decay. The leading edges of the first peaks are substantially less sharp compared to those observed for oxygenated environments. Most profiles have small but identifiable oscillations in the tail of the profile. The oscillations are overlapped with decay in the overall emission intensity.

Inspecting the water profiles shown in Figure 2.7, it appears that the initial peaks are substantially greater in intensity than the rest of the emission signal. The leading edges of the initial peaks are sharper than in CO_2. The overall duration of the initial peaks is comparable to the estimated time the particles are crossing the laser beam. Thus, it appears that immediately after the laser source is removed, the emission drops rapidly to a very low level, which is substantially lower than that observed for any of the other environments. However, the emission remains reliably above the baseline level for a while, suggesting a relatively steady exothermic reaction that is accompanied by emission that is much weaker compared to reactions in O_2 and CO_2.

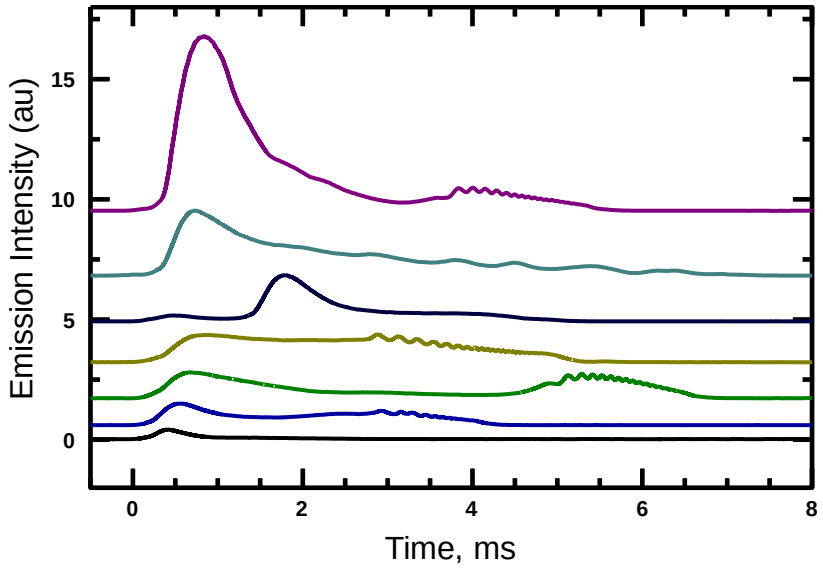

Figure 2.6 Emission profiles for Al particles burning in a 73/27 CO_2/N_2 mixture.

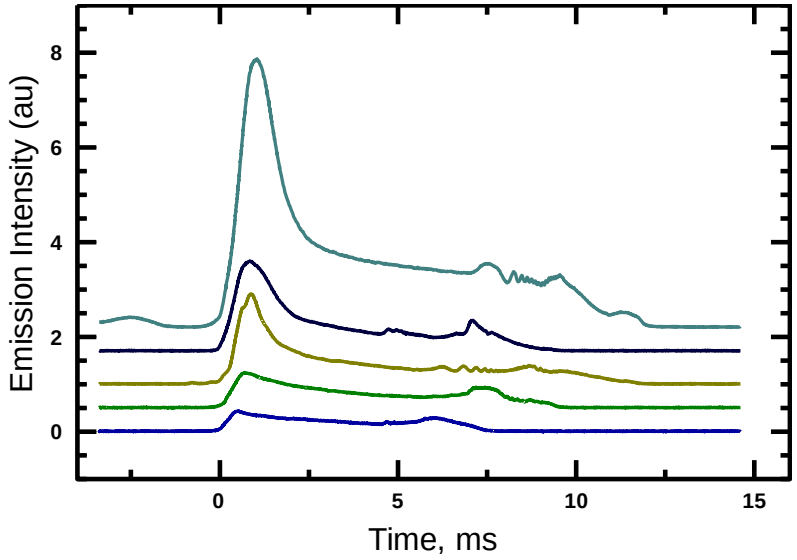

Figure 2.7 Emission profiles for Al particles burning in a 10/90 O_2/N_2 mixture.

2.3.2 Burn Times

Burn times are presented in Figures 2.8-2.12, where all experimental data points are shown. Each point represents a particle, for which the diameter is measured from the scattered pulse sequence, and the burn time is inferred from the duration of the correlated emission pulse. In other words, each point represents a pair of pulses measuring particle

emission and scattered light, which are correlated in time to ensure that both pulses were produced by the same particle. As discussed above, the majority of the measured pulse durations do not represent the burn times of interest. Only the longest measured pulse durations for each particle size can be interpreted as the burn times for a self-sustained particle combustion that was not assisted by laser. For each set of experimental data points, a trend line showing the D^n fit is also shown as a solid line. The fit is obtained for data points representing the longest measured pulse durations for each particle size range. The particle size ranges and the respective longest pulse durations are selected manually and somewhat subjectively from all the measured data points. The points used to calculate the trend line are shown as filled symbols while the rest of the experimental data points are presented as open symbols. Note that each data point used in the "power-law" fits, was inspected additionally to confirm that for each such matched pair of emission and scattered light peaks both peaks were well separated from their neighbors, were clearly above the noise level, and that the emission profile was typical of aluminum combustion in the respective environment. Despite an elaborate automated peak processing routine described in reference [16], some outlier points were still identified by this additional inspection, which were likely caused by ignition of agglomerated particles or particles closely following each other in the jet. Such outlier points were removed from Figures 2.8-2.12.

In addition to the experimental points and solid trend lines, three dashed lines are also shown for each plot. The dashed lines show particle burn times predicted for each specific environment as a function of the particle diameter using three different D^n trends

reported in the literature for aluminum combustion. For all trends, the particle diameter, *D*, is entered in mm and the burn time, τ_b, is calculated in ms.

The first trend, given by Equation 2.1, comes from a review of published experimental results, primarily for coarser Al particles, compiled by M. Beckstead [21].

$$\tau_b = \frac{7.35D^{1.8}}{\left(C_{O_2} + 0.6C_{H_2O} + 0.22C_{CO_2}\right)P^{0.1}T^{0.2}} \tag{2.1}$$

In Equation 1.1 and below, *C* is the concentrations of oxidizer given by the respective subscript, *P* is pressure, and *T* is the environment temperature.

The second trend is described by the set of equations found in Equations 2.2 and was proposed by N. Glumac et al. [6] based on measurements using aerosolized Al particles ignited in a shock tube. These measurements identified average combustion times of narrowly size-classified Al powders. The burn times were obtained from the widths of the optical emission peaks produced by the powders ignited in a gas heated by the shock wave.

$$\begin{aligned} \tau_b &= a_o C_{OX}^{a_1}\left(\frac{P}{P_0}\right)^{a_2} D^n \\ n &= 2\exp\left(-4.3C_{OX}\right)\left(\frac{P}{P_0}\right)^{-0.3} \\ \tau_{b,mix} &= \left(\sum_{i=1}^{n}\frac{1}{\tau_{b,i}}\right)^{-1} \end{aligned} \tag{2.2}$$

Similarly to Equation 2.1, Equation 2.2 describes effects of oxidizer concentration and ambient pressure. The reference pressure that should be used in Equation 2.2 is P_0=8.5 atm. The effect of the oxidizer type is given by the choice of constants a_0, a_1, and a_2, as described in Table 2.2. Unlike Equation 2.1, there is no effect of ambient temperature in Equation 2.2. However, it should be noted that the measurements used to obtain Equation 2.2 were performed in hot ambient gases.

Table 2.2 Selection of Constants as a Function of Oxidizer for Use in Equation 2.2 [6]

Oxidizer	***a₀, ms***	***a₁***	***a₂***
O_2	200	0.5	-0.5
CO_2	500	0.6	0.3
H_2O	86	-1.7	0.75

Finally, the third trend used for reference calculations of the burn time is given by Equation 2.3 and was taken from reference [22] by Shoshin and Dreizin, where the particle burn times were measured using a lifted laminar flame burner. The experiments were performed in air only, so Equation 2.3 does not take into account effects of ambient pressure, temperature, oxidizer type or concentration.

$$\tau_b = 310 \cdot D \tag{2.3}$$

Results for burn time for aluminum in the 10% oxygen mixture are shown in Figure 2.8. Both Equations 2.1 and 2.3 substantially underestimate the particle burn times, while Equation 2.2 predict much longer burn times than observed in experiments. Note that experimental points appear for particles greater than about 3 μm, indicating that the smaller particles were difficult to identify based on the measured scattered light

pulses. This restriction is due to a smaller peak to noise ratio for the scattered signal from the small scattered light peaks produced by small particles.

A relatively weak increase in the burn time for increased particle sizes is observed and it is reasonably well described by a $D^{0.32}$ trend line.

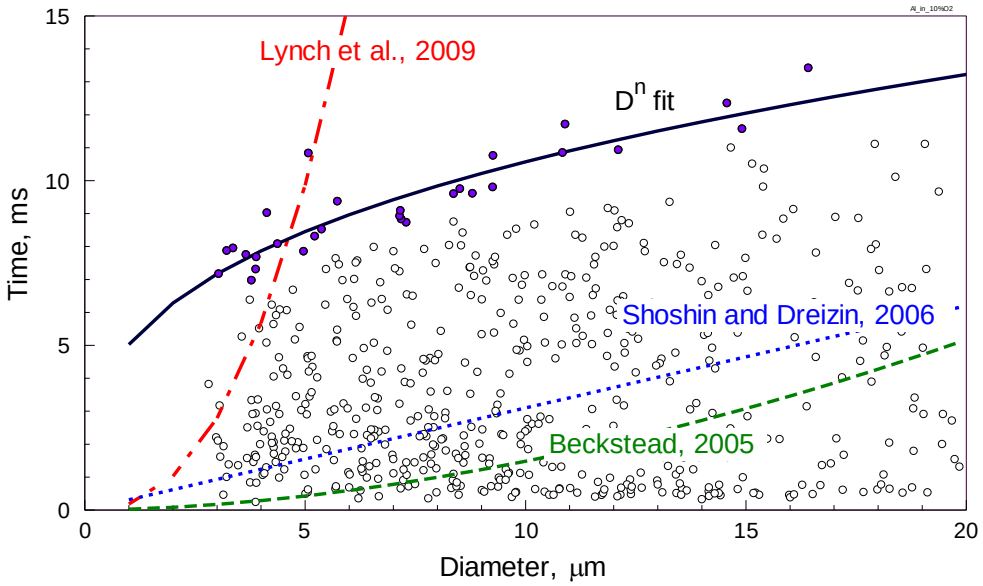

Figure 2.8 Particle combustion times as a function of the particle diameters for Al burning in a 10/90 O_2/N_2 mixture. Here and in Figures 2.9-2.12, open and closed symbols: experimental points; closed symbols used for the D^n fit shown by solid line (n=0.32). Dashed lines show D^n trends reported in the literature (see text).

As already noted from examination of individual emission traces, the burn times are substantially reduced when the concentration of oxygen is increased to 21% as shown in Figure 2.9. For this case, Equation 2.1 continues to under-predict the particle burn times and Equations 2.2 still predict longer burn times than observed experimentally. It is interesting that Equation 2.3 appears to work rather well and for the set of data available the predicted trend nearly coincides with the directly calculated best match line.

The results for the 40% oxygen mixtures are shown in Figure 2.10. It is interesting that despite substantially increased oxygen concentration, the burn times do not decrease noticeably compared to the 21% oxygen case. Calculations by both

Equations 2.1 and 2.2 for this case predict shorter burn times than observed experimentally. Calculation by Equation 2.3 somewhat over-predicts the observed burn times and the curve directly matching the experimental data is described by a $D^{0.57}$ trend line.

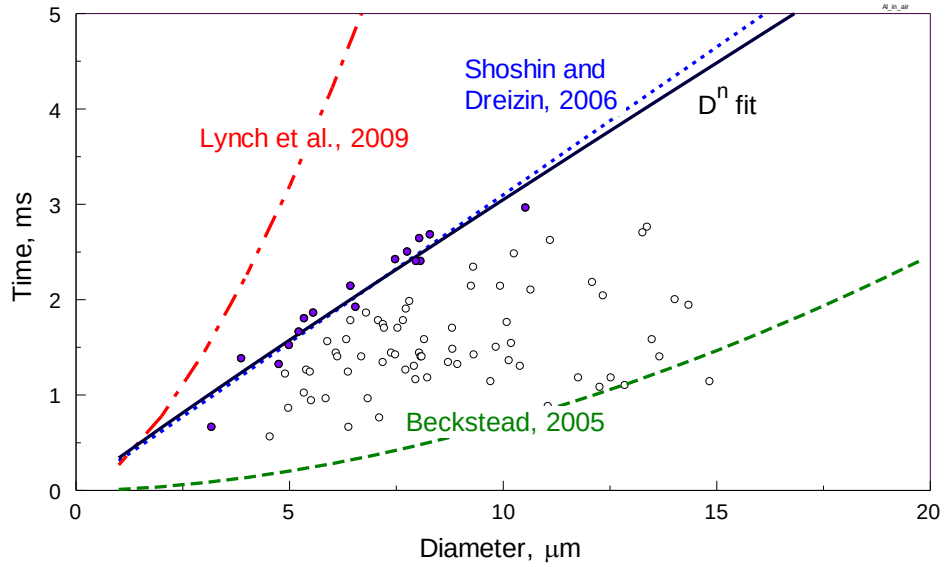

Figure 2.9 Particle combustion times as a function of the particle diameters for Al burning in a 21/79 O_2/N_2 mixture (air). D^n fit is shown by a solid line (n=0.95).

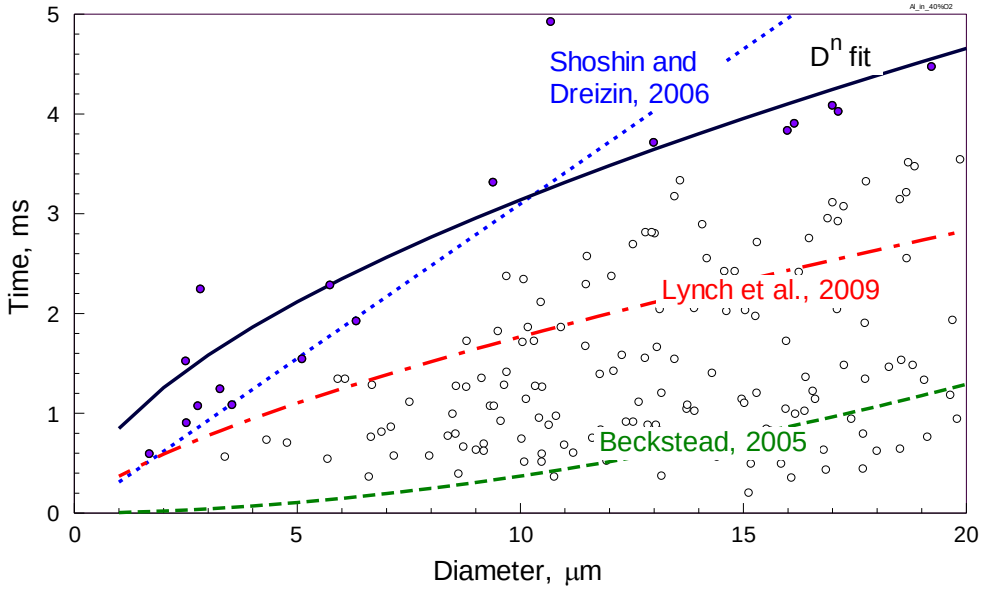

Figure 2.10 Particle combustion times as a function of the particle diameters for Al burning in a 40/60 O_2/N_2 mixture. D^n fit is shown by a solid line (n=0.57).

Burn times for aluminum particles in 73% CO_2 mixture are shown in Figure 2.11 and are quite long, despite a very high concentration of the oxidizing gas. All reported trends, Equations 2.1-2.3, substantially under-predict the combustion times as compared to the current measurements. The experiments are described by a trend line similar to that used to describe the data for the 10% O_2 mixture.

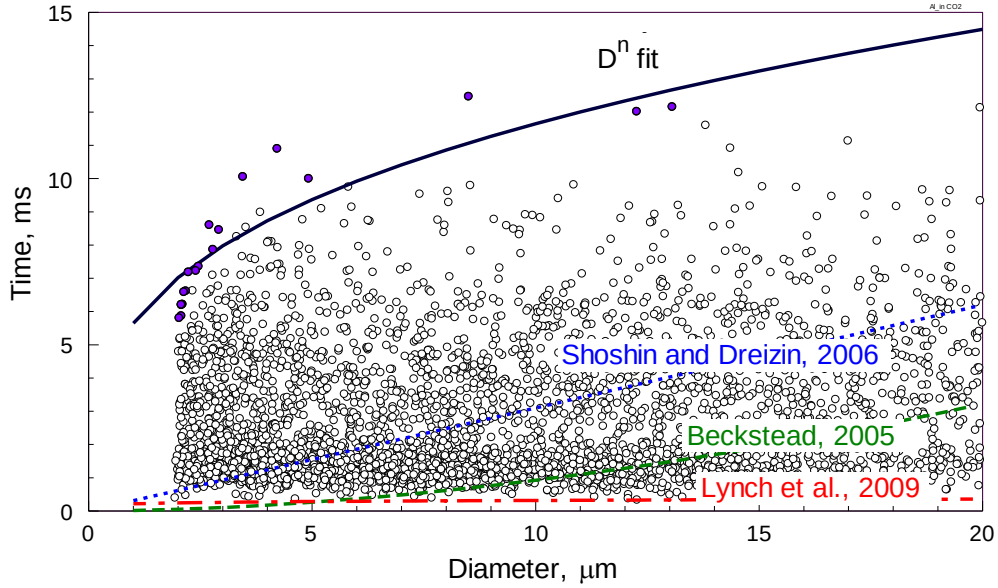

Figure 2.11 Particle combustion times as a function of the particle diameters for Al burning in a 73/27 CO_2/N_2 mixture. D^n fit is shown by a solid line (n=0.32).

Finally, for aluminum combustion in 77% of H_2O vapor, the burn times are somewhat shorter than for CO_2, but longer than in oxygen. Once again, all reported trends significantly underestimate the combustion times.

Table 2.3 gives the exponents and pre-exponents for all the power law fitting functions used for these experiments. It is interesting that in no case an exponent greater than 1 is observed. At the same time, very small exponents, around 0.3, are observed for three cases: H_2O, CO_2 and 10% O_2 environments.

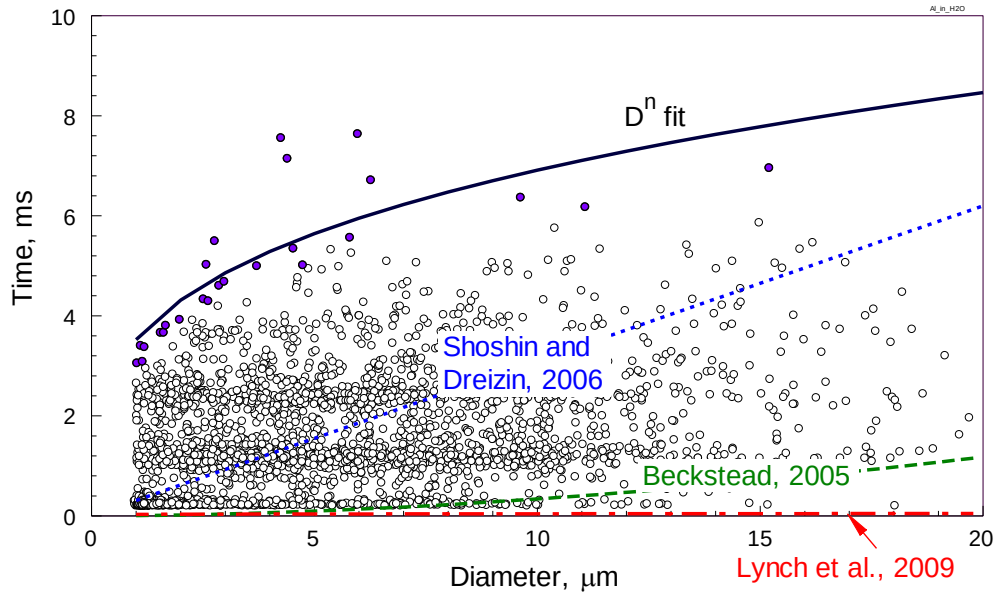

Figure 2.12 Particle combustion times as a function of the particle diameters for Al burning in a 77/23 H_2O/N_2 mixture. D^n fit is shown by a solid line (n=0.29).

2.4 Discussion

This work presents, for the first time, detailed emission traces produced by individual burning aluminum particles in the size range of 3-20 μm. Previously, similar traces were reported for much larger particles burning in air and other environments, e.g., [13, 27, 28]. Previous work established that multiple peaks and oscillatory emission patterns produced by burning aluminum particles are associated with non-uniformities in the particle composition developed during combustion. Specifically, pure Al particles become saturated with the dissolved combustion products (e.g., oxidized Al species, nitrogen oxides, and more complex compounds formed in presence of CO_2 and other oxidizers) which results in separation of molten aluminum into two or more liquid solutions [13, 27, 28, 37]. Each solution component evaporates at a different rate resulting in an asymmetric flame and associated oscillatory emission pattern. Furthermore, continuing oxidation results in the formation of oxide caps producing yet

another oscillatory emission pattern, typically observed by the end of combustion. The described above processes were identified from comparisons between the particle emission profiles and morphologies and compositions of aluminum particles rapidly quenched at different stages of their combustion [13, 37]. Such quenching experiments and analyses of the particle morphologies are extremely difficult for finer aluminum particles commonly used in practical applications. However, current results suggest that the emission profiles for finer Al particles are qualitatively identical to those observed earlier for greater size particles, suggesting that the same combustion processes occur and determine the rate of metal consumption and associated heat release. Specifically, current observations of oscillatory emission patterns occurring in a sequence similar to that reported earlier for coarse Al particles, suggest that heterogeneous processes play a substantial role in Al combustion even in environments comprising 40 % O_2.

The particle emission profiles measured in experiments performed with H_2O as an oxidizer are qualitatively different from those recorded in other environments. A very low and relatively steady level of emission suggests that the vapor phase flame is very weak or non-existent, while the particle continues to react exothermically, remaining weakly incandescent. This emission behavior suggests a surface reaction, suggesting that Al combustion in H_2O is primarily heterogeneous. Interestingly, recent estimates presented in reference [38] indicated that a relatively low heat release for aluminum oxidation by water is insufficient for maintaining a standoff vapor-phase flame for micron-sized particles burning in room temperature environment, as in the present experiments. Thus, present observations indicative of the surface combustion for aluminum particles in H_2O are consistent with the predictions of reference [38].

Reviewing measured particle burn times as compared to the predictions of Equations 2.1-2.3, it becomes clear that none of the currently reported trends are suitable for practically useful and reasonably accurate prediction. In particular, the discrepancies are greatest when the experimental conditions are different from those used to establish the specific trend. In that sense, the best match fits found in this work and summarized in Table 2.3 are as limited as any other proposed trends. As with other trends, they are only suitable for calculation of the particle burn times for experimental conditions similar to those used to find the respective relations.

More specifically, it is suggested that Equation 2.1 based on Beckstead's analysis of multiple experimental results is heavily biased to experiments with much larger particles. Thus, estimating burn times for finer particle sizes is challenging, and, as observed here, results in substantial errors. Equation 2.2 is based on experiments performed at relatively high pressures and temperatures. It is also worth noting that Equation 2.2 are based on the measurement of the emission peak produced by a group of burning particles, so that the peak duration is dominated by larger particle sizes, even if the number of smaller particles is significant. Alternatively, only smaller particles could have ignited in selected shock tube experiments resulting in very short combustion peaks, whereas larger particle present in the system may not have ignited. Corrections for such effects and for the effect of high environment temperature are difficult, and without such corrections Equation 2.2 do not predict combustion times accurately. Finally, Equation 2.3 is very simplistic and does not account for oxidizer concentration, type, or any other experimental condition. In fact it is somewhat surprising how well it described the current experimental data for mixtures with 21% O_2, for which it was initially proposed. Because

Equation 2.3 was obtained based on aerosol combustion experiments, it is suggested that the particle interaction effects in Al aerosol combustion are relatively weak so that the particle burn rates for single particles and particles burning in an aerosol effectively coincide with each other. Alternately, the particle number density could have been below the levels where such effects would be measureable.

Finally, to comment on the specific burn times measured in this work for different environments, it is interesting to compare these times to one another. To streamline such a comparison, all "best fit" trend lines are plotted together in Figure 2.13. A small difference between the burn times measured for Al in 21% and 40% O_2 mixtures is remarkable and indicative that in these environments, the aluminum combustion may be relatively well described by a heat transfer limited droplet combustion model with a stand-off flame [39], where the rate of combustion is determined by the transfer number *B*, which is not affected by the oxidizer concentration and is defined as:

$$B = \frac{\Delta h_c / \upsilon + C_p \left(T - T_{boil}\right)}{L} \tag{2.4}$$

where Δh is the heat of oxidation, L is the latent heat of evaporation, C_p is specific heat, υ is the stoichiometric coefficient, and T and T_{boil} are the temperatures of the hot environment (assumed here to be equal to the flame temperature) and particle surface, respectively. It is somewhat unexpected that a bit longer burn times are anticipated for the particles less than 10 μm at 40% O_2 as compared to 21% O_2. This effect may simply represent an experimental uncertainty. It is also possible that the dimensions of extinguished particles are reduced at greater oxygen concentrations, resulting in

somewhat longer overall reaction times. Additional measurements and, possibly, analyses of the combustion products would be needed to address this issue in the future.

Table 2.3 Fitting Coefficients for Particle Diameter Power Law Fitting Equation: $\tau_{burn} = a \cdot D^n$

Gas environment (remainder N_2)	*a*	*n*	Correlation Coefficient, r^2
10% Oxygen	5.03	0.32	0.82
21% Oxygen (Air)	0.34	0.95	0.93
40% Oxygen	0.85	0.57	0.81
73% Carbon Dioxide	5.65	0.32	0.86
77% Water Vapor	3.52	0.29	0.68

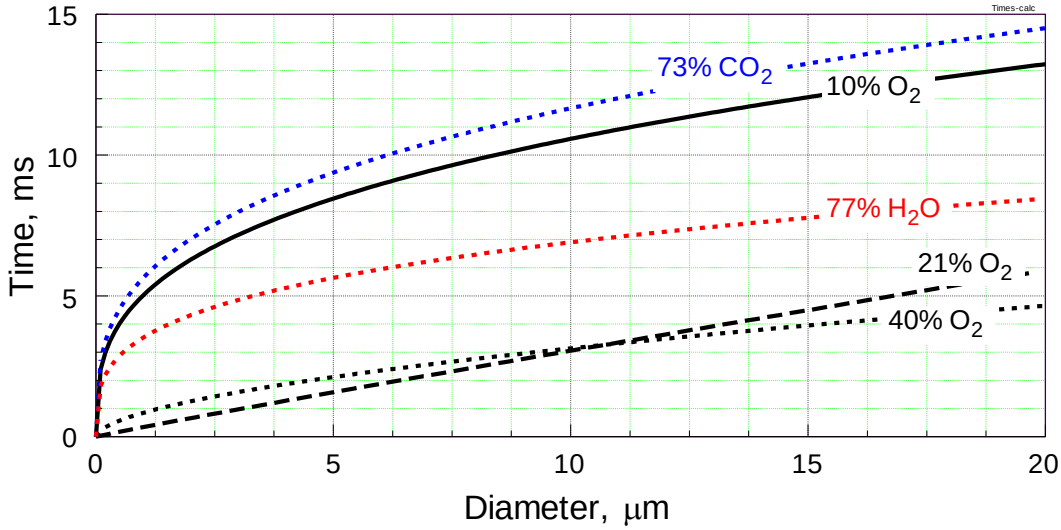

Figure 2.13 Calculated burn times based on the best matches with experimental results presented in Figures 2.8 – 2.12 for aluminum particle combustion in different oxidizing environments.

For reduced oxygen concentration, the combustion times increase substantially, suggesting that a different rate limiting process is at play. Most likely this rate-limiting process is the heterogeneous oxidation occurring on the particle surface. The overall emission level also decreased suggesting a reduction in the size of the vapor phase flame and an increasing contribution from surface reaction processes.

For CO_2 and H_2O environments, the role of surface processes is expected to be substantial for micron-sized particles, based on the heat balance estimates presented in reference [38]. Respectively, long particle combustion times are measured despite high oxidizer concentrations in both cases. The significance of surface processes is particularly pronounced for combustion in H_2O as discussed above. Therefore, aluminum combustion models taking such processes into account need to be developed and validated by comparisons with the current and future experiments. It is interesting that the exponent close to 0.3 was found to describe the observed trends for all cases when heterogeneous reactions deem to be important. While this value of exponent indicates a very weak effect of particle size on the burn time, it can also indicate that particles of different dimensions combust in different regimes. Specifically, heterogeneous reactions, which occur at lower temperatures and generally lower rates, prevail for smaller particles, resulting in extended burn times. As the particle size increases, vapor phase reactions play an increasingly greater role, resulting in a faster burn and thus shorter burn times. Note that results summarized in Figure 2.13 describe experiments performed at atmospheric pressure. In many practical systems involving metal combustion the pressures are elevated, so that the particle dimensions for which the vapor phase reactions are important will be smaller than in this work. It is anticipated that descriptive models of metal combustion dynamics can be developed and validated based on measurements similar to those presented in this paper. These combustion dynamics should be incorporated into the models so that the effects of pressure and environment composition could be predicted with reasonable accuracy.

2.5 Conclusions

A new experimental setup enables measurements of optical emission signatures and combustion times for individually sized metal particles with diameters between 3 and 20 μm. The measurements can be carried out in various oxidizing environments, including oxygen, carbon dioxide, and water mixed with nitrogen or other inert diluents. Extending the set of environments using mixed oxidizers and, possibly, elevated pressure, are possible avenues of future work.

Optical signatures of individual micron-sized aluminum particles burning in different environments show characteristic oscillatory patterns previously observed for much larger particles. Such optical signatures highlight the importance of the heterogeneous processes in aluminum combustion. Heterogeneous reactions result in variation of surface properties of the burning droplets, which, in turn, cause formation of asymmetric flames and repeatable changes in particle emission intensities. For aluminum burning in water vapor, the optical signature of the particle is substantially weaker than in other environments, possibly indicating a primarily surface oxidation.

Results presented in this paper show that the current simplified D^n correlations for aluminum combustion time reported in the literature cannot be usefully applied for the conditions beyond the narrow ranges, for which such correlations were developed initially. It is observed that for oxygenated environments with oxygen concentrations in excess of 21%, the effect of oxygen concentration on combustion time of micron-sized aluminum particles is weak. However, combustion times increase substantially for lower oxygen concentrations. Aluminum particle combustion times are generally longer than predicted for experiments with water and carbon dioxide oxidizers. For all environments,

the observed effect of particle size is relatively weak and the exponents in the descriptive D^n relations appropriate for the current experiments vary approximately from 0.3 to 1. An exponent close to 0.3 describes well the burn-times for aluminum in oxidizing environments for which heterogeneous reactions appear to dominate.

CHAPTER 3

TEMPERATURES, MOLECULAR ALO EMISION, AND BURN TIMES OF MICRON-SIZED ALUMINUM PARTICLES BURNING IN OXYGENATED ENVIRONMENTS

Experimental data describing combustion of micron-sized aluminum particles as a function of their size are limited. Often combustion characteristics are derived indirectly, from experiments with aerosolized powder clouds. In a recently developed experiment, micron-sized particles cross two laser beams. When each particle crosses the first, low-power laser, it produces a scattered light pulse proportional to the particle diameter. The second, powerful CO_2 laser beam ignites the particle. The optical emission pulse of the burning particle is correlated with its scattered light pulse, so that the combustion characteristics are directly correlated with the size for each particle. In this work, emission signatures of the ignited Al particles are recorded using an array of filtered photomultipliers to enable optical pyrometry and evaluate the molecular AlO emission. Processing of the generated data for multiple particles is streamlined. Experiments are performed with spherical aluminum powder burning in atmospheric pressure O_2/N_2 gas mixtures with the oxygen concentrations of 10, 15, and 21% (air). In air, the AlO emission peaks prior to the maximum in the overall emission intensity, and the latter occur before the maximum of the particle temperature. The temperatures at which particles burn steadily increase with particle size for particles less than 7.4 μm. For coarser particles, the flame temperature remains constant at about 3040 K. In the gas mixture with 15% O_2, the flame temperatures are observed to increase with particle size for the entire range of particle sizes considered, 2-20 μm. At 10% O_2, the flame temperatures are significantly lower, close to 2000 K for all particles. The intensity of

AlO emission decays at lower oxygen concentrations; however, it remains discernible for all environments. The results of this study are expected to be useful for constructing the Al combustion models relaxing the assumption of the steady state burning.

3.1 Introduction

Aluminum powder is a widely used fuel additive in solid propellants, explosives, and pyrotechnics [1-3]. Efforts to understand the combustion reactions for aluminum, to describe quantitatively and, ultimately, optimize its combustion dynamics for specific applications have been active for several decades. One parameter of practical interest is the particle burn time, τ_b. Stemming from studies for combustion of liquid droplets [21], the semi-phenomenological expression of burn time is typically presented as a power law $\tau_b = a \cdot D_p^n$ with a functional dependence on the particle diameter, D_p. Commonly, the coefficient a and exponent n are determined empirically. Several authors presented expressions for these parameters for different oxidizing environments and external temperatures and pressures [15, 16, 21, 33, 40]. All such descriptions effectively reduce particle combustion to a steady state process neglecting changes occurring in the burn rate and corresponding heat release as a function of time.

Most of the experimental data used to develop empirical correlations for particle burn times were based on experiments with aerosolized Al powder clouds or jets [6, 30, 33, 40-42] or with coarse, 100 μm or greater single Al particles [13, 15, 26, 27]. For particles less than 20 μm employed in many practical formulations, data on single particle combustion are limited. This size range is particularly interesting because the combustion mode is expected to transition from the gas-phase diffusion limited combustion for

coarser particles to the combustion regime limited by the surface reaction kinetics for finer particles [6, 11, 15, 41].

Different mathematical descriptions for aluminum particle combustion processes have been developed recently [3, 11, 12, 38]; however, all current models assume combustion to occur steadily, neglecting substantial changes known to occur in the reaction mechanisms while the particle is burning out [13]. Comparisons between predictions and experiments continue to use overall combustion times, which could be misleading considering the substantial changes that can occur in the aluminum particle burn rate when its size is decreasing and when the size of the growing oxide cap becomes larger.

This study continues an effort presented in reference [15] aimed at developing an experimental method for direct characterization of combustion behavior of individual, micron-sized metal particles. Initial experiments were limited to finding the total particle burn times as a function of their size, so that results could be compared to existing empirical correlations. In this effort, the diagnostics are extended to include time-resolved optical pyrometry and monitoring molecular AlO emission for burning particles. The data processing is streamlined and results for Al combustion in oxygenated environments with different oxygen concentrations are presented and discussed.

3.2 Experimental

3.2.1 Apparatus

Individual metal particles are fed by a gas flow into a CO_2 laser beam where they are ignited. Before particles cross the CO_2 laser beam, they cross a beam of a 785 nm, 30 mW laser and the scattered light pulses are used to measure particle sizes. Particle velocities are measured using an additional modulated laser sheet [16]. Previous publications [15, 16] described the apparatus used for this experiment. In this project, the setup was modified to enable optical temperature measurements, as shown in Figure 3.1.

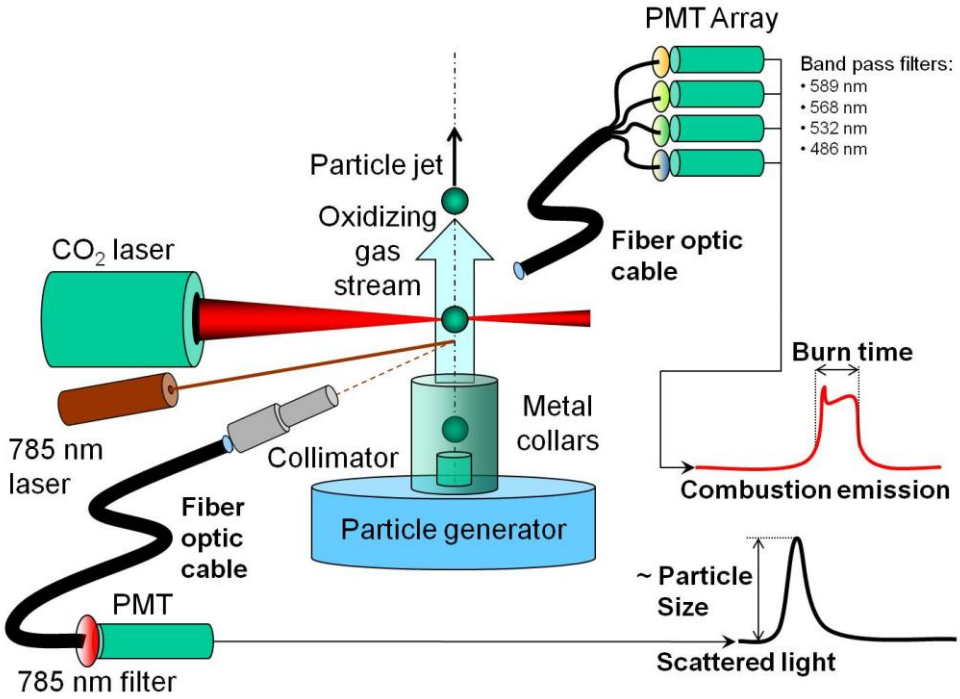

Figure 3.1 Experimental apparatus and diagnostics to obtain particle size and emission pulse correlation.

Light emitted by ignited particles passes through a quad-furcated fiber optic bundle leading to an array of four photomultiplier tubes (PMT, Hamamatsu H3164-10), each equipped with an interference filter. A 486 nm filter is used to detect AlO molecular emission. 532, 568, and 589 nm filters are used for optical pyrometry.

Each of the four PMTs was calibrated using a current-stabilized tungsten lamp and an irradiance calibrated spectrometer (StellarNet EPP2000). The spectrometer manufacturer provided the calibration of the CCD array, with a quartz fiber optic and a cosine filter installed. For PMT calibration, a spectrum of the current-stabilized tungsten lamp was measured. Therefore, the true lamp emission intensity for each wavelength was obtained without the need to know the emissivity of the ribbon. Then, the spectrometer fiber optic cable was replaced with that transmitting light to the filtered PMT's, so that the location of the inlet window facing the lamp did not change. The signal measured by each of the filtered PMT was then related to the respective true light intensities, so that the sensitivity factor for each PMT was obtained. The fiber optic transmission curve was not used assuming it be the identical for each fiber bundle of the quad-furcated cable. For temperature measurements, measured light intensity ratios were used and the emitters were assumed to be gray bodies.

For extended calibration, the tungsten lamp was operated at several fixed current levels so that responsivity curves for each filtered PMT were obtained. In addition, the PMT gain curves were obtained measuring the variation of the PMT signal as a function of the applied PMT voltage at a fixed irradiance. To cross-check the accuracy of the gain function fit to the data, a set of neutral density filters was used to measure the response of each PMT under a wide range of light intensities (>3 decades). The gain curves accurately predicted (to within a few percent) the PMT output voltages. This calibration allowed us to measure the aluminum emission over a wide dynamic range of light intensities.

Spherical aluminum powder used in this project was from Alfa Aesar, nominal size 10-14 μm. The powder is fed into the laser beam using an electro-static aerosol generator [16, 33]. Experiments are conducted at 1 atm in three different room-temperature O_2/N_2 gas flows with oxygen concentrations of 10, 15 and 21 % (Air).

3.2.2 Data Processing

The first processing step is to compare the powder particle size distribution measured by a commercial device based on the low-angle laser light scattering, Beckman-Coulter LS230, with that implied from the amplitudes of the scattered 785 nm light pulses measured in this experiment. The best match between the two size distributions is obtained by varying a single scaling factor of the scattered light peak heights. An adjustment in the scaling factor is required for each powder, which can be explained by differences in the particle shapes and surface morphologies affecting the intensity of the scattered light. The comparison between the two size distributions for the Al powder used in this project is shown in Figure 3.2. The match is imperfect but salient features of the powder size distributions are represented well.

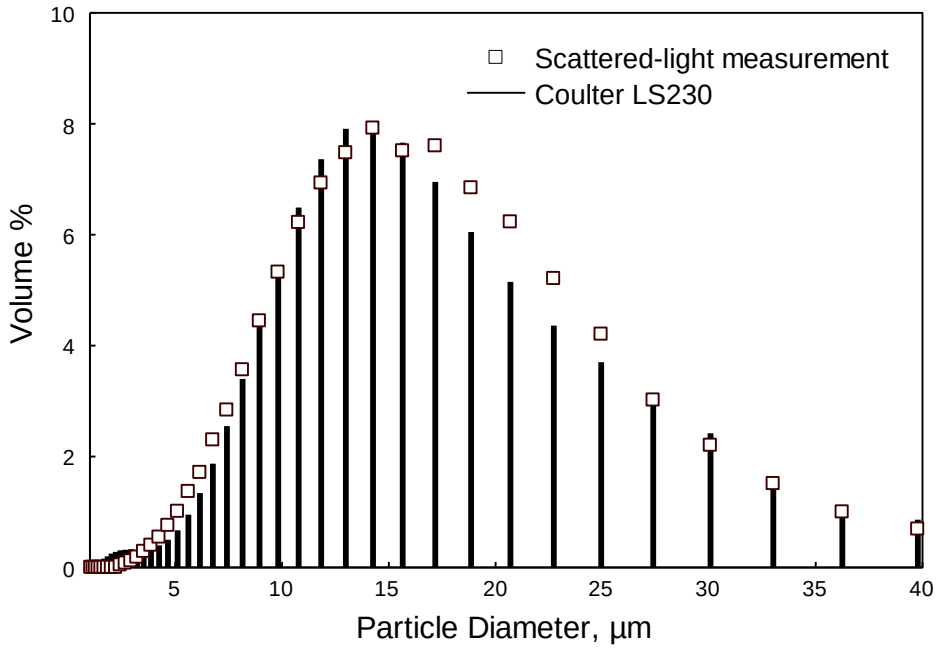

Figure 3.2 Particle size distribution measured in the commercial device (Coulter LS230) and the scattered-light measurement for aluminum.

The second processing step is to correlate the two measured pulse sequences: a sequence of scattered light pulses and a sequence of pulses produced by heated and ignited incandescent particles. For each particle, the scattered light pulse and its emission pulse are separated by the period required for the particle to travel between the two laser beams. This time is known approximately based on the measured particle velocities. For different particles, this time can vary in a certain range, depending on the individual particle velocities. In the signal processing procedure, the time shift between the two measured pulse sequences is varied to achieve the maximum number of matches between pulses. The time shift must be close to that anticipated from the measured particle velocities. The pairs of pulses shifted relative to each other with that time shift (within a selected narrow time window accounting for the variation in individual particle velocities) are identified for further processing and are assumed to represent individual particles.

In the next processing step, pairs of pulses that overlap in time or immediately follow one another, and thus could represent interacting particles, are removed from further processing.

For each particle, its size is correlated with the measured emission time and combustion temperatures are determined. As described in detail elsewhere [15], only the longest emission times measured for each range of particle sizes are representative of burn times of interest. Shorter emission light pulses are produced by particles that are heated but not ignited in the laser beam and by particles that ignite well before exiting the laser beam. In the latter case, a portion of particle combustion occurred within the laser beam and thus the reaction was assisted by laser heating. The longest emission pulses are produced by particles that ignite just before exiting from the laser beam, so that their combustion is not affected by additional laser heating. Previously, the longest emission pulses were selected manually, which could have resulted in a somewhat subjective choice [15, 16]. In this project, the longest emission times are selected following a consistent procedure. Initially, the range of particle sizes for which the measured emission times were available was broken down into 4 size bins. For each particle size bin, cumulative distributions for measured emission times are plotted. Only the particles for which the emission times are in the top several % for that bin are finally selected for further processing. In these experiments, the particles with burn times in the range of 97.5-100 % were selected. For these selected particles, burn times as a function of their size are found, particle combustion temperatures are measured, and AlO emission traces are recorded.

3.3 Results

A representative photograph of burning aluminum particle streaks in air is shown in Figure 3.3. The flow settings are selected so that the measured average particle velocities are close to 0.5 m/s. Multiple short streaks are observed, likely produced by particles that are heated but not ignited or heated and partially burnt in the laser beam and are discounted from the data processing. Some of the long streaks correspond to particles moving in random directions after exiting the laser beam. Those particles are likely ignited and partially burned in the laser beam; they also should not be included in the data processing. Finally, longest streaks with initially vertical particle velocities are likely to represent particles ignited when exiting from the CO_2 laser beam; these particles are included into the present analysis. Initial portions of the trajectories for the particles are straight and bright followed by weaker streaks with sharp changes in the particle direction.

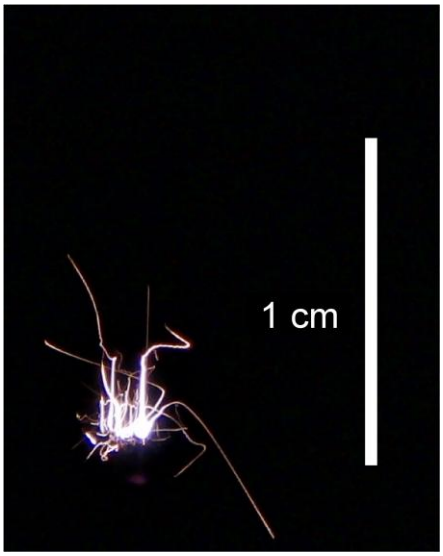

Figure 3.3 Photograph of burning aluminum particle streaks in air.

Selection of particles with the longest measured emission times representing meaningful burn times, not assisted by laser heating, is illustrated in Figure 3.4 for an experiment with Al particles burning in air. For this specific example, the entire range of particle sizes, for which matching pairs of emission and light scattering pulses were identified, was 2-30 μm. This range was divided into four bins, 2-6, 6-10, 10-14, and 14-30 μm. For each size bin, normalized cumulative distributions of the particle emission durations were obtained, these distributions are shown in Figure 3.4.

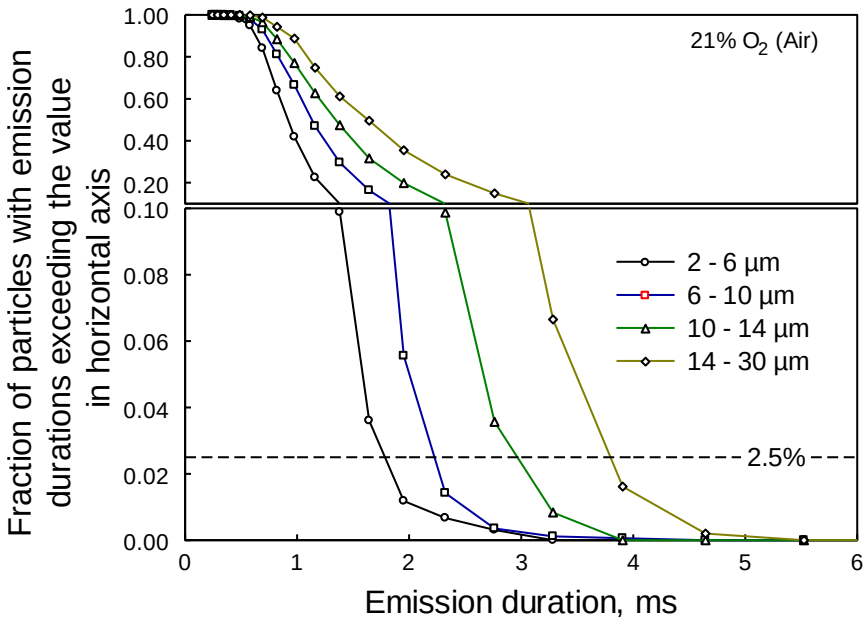

Figure 3.4 Normalized cumulative distributions of emission durations for Al particles burning in air.

As the distributions show, no particles emitted light longer than 6 ms and almost no emission pulses were shorter than 1 ms. For clarity, the vertical scale in Figure 3.4 is expanded for the fractions less than 0.1, i.e., for the particles with the emission durations in the top 10 %. As expected, particles with larger sizes generally exhibit longer emission durations. The cutoff of 2.5 % was selected, somewhat arbitrarily, as shown by the horizontal dashed line in Figure 3.4, so that the cumulative distributions are meaningfully

separated from one another while a reasonable numbers of particles are available in each size bin. Greater cutoff thresholds lead to shorter inferred burn times for the same particle sizes; for example an increase in the threshold up to 10 % for a typical data set results in an almost 20% reduction in the emission time for a specified particle size range. However, the effect of particle size on the emission time remains essentially unchanged.

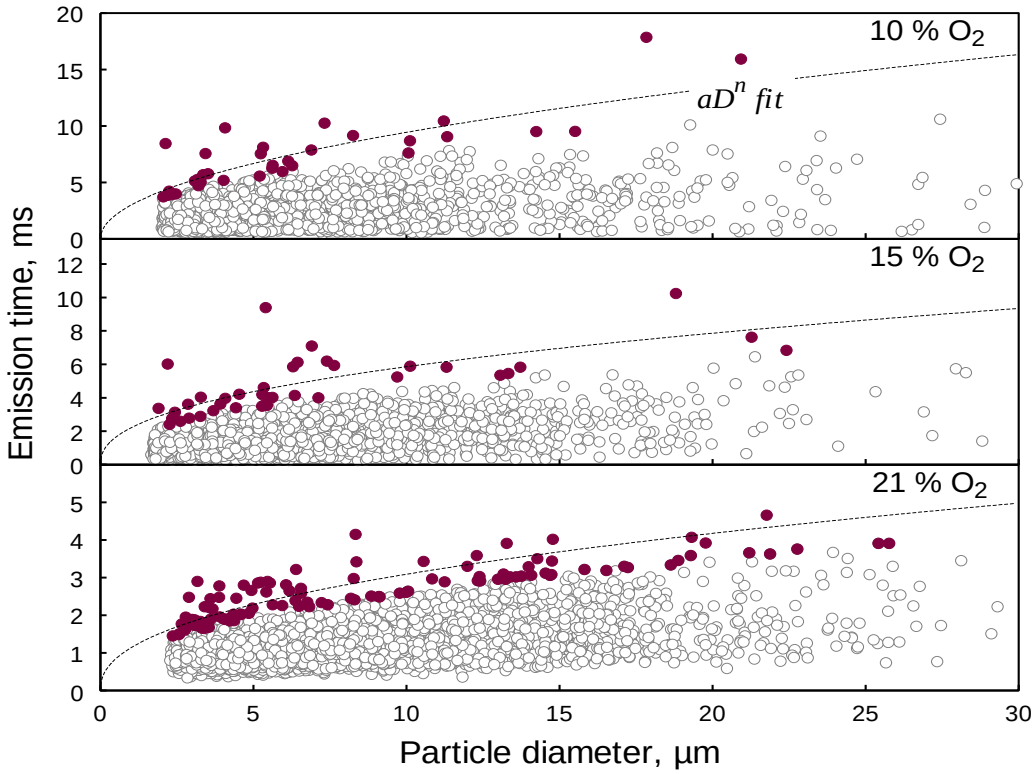

Figure 3.5 Burn times as a function of particle size for aluminum particles ignited in different O_2/N_2 gas mixtures.

Scatter plots shown in Figure 3.5 present the matching pairs of the emission and light scattered pulses identified as described above for aluminum powder in three environments with different oxygen concentrations. No data points are available for particles less than 2 µm as the light scattered pulses were comparable to the signal noise. Filled symbols in Figure 3.5 represent the subsets of all data points with emission times

within the top 2.5 %, identified as illustrated in Figure 3.4. These are the points used to determine the effect of particle size on its burn time and to analyze the particle combustion temperatures and AlO emission signatures.

Following earlier work, a trend for the burn time as a function of the particle size was obtained for each environment in the form of $\tau_b = a \cdot D^n$. The parameters *a* and *n* corresponding to the best fit for each environment are shown in Table 3.1. The fitting curves are also shown in Figure 3.5. The exponent values in the range of 0.4-0.5 for pure aluminum are consistent with empirical exponents reported in some of the earlier work [6]. Note that the D^n fits presented here do not coincide with those reported in our previous paper [16] in which the same experimental setup was used. While the trends suggested based on the previously reported data sets [15] describe the present data reasonably well, the present experimental data sets are more extensive and thus offer a somewhat better assessment of the D^n trend valid in the range of particle sizes of 2-20 μm. Most importantly, it should be emphasized that all such descriptions imply a steady particle burn rate and effectively neglect any changes in the particle combustion regime. Thus, the significance of any D^n type trends is very limited and using such trends to describe particle combustion in practical systems is not recommended.

Table 3.1 Empirically-based Parameters for the $\tau_b = aD^n$ Fit Shown in Figure 3.5 for the Aluminum Particle Burn Times Measured in Different Environments

	% O_2	***a***	***n***	**Correlation, r^2**
	10	2.99	0.5	0.62
Aluminum	15	2.21	0.42	0.49
	21	1.29	0.35	0.76

Figure 3.6 shows individual emission traces and temperature profiles for three aluminum particles burning in different O_2/N_2 gas mixtures. All three particles were selected with approximately 6 μm diameter, so the differences in the emission durations between the traces in Figure 3.6 represent the effect of the oxidizing environment. The temperatures shown were calculated from the ratio of PMT signals acquired through 589 nm and 532 nm filters. This ratio was more sensitive to changes in the burning particle temperature and yielded more reliable temperature reading than the others, using the signal filtered at 568 nm.

Emission traces are qualitatively similar to those presented earlier [15]. An initial peak is followed by a decay, a plateau, which is poorly distinguished in some traces, and final intensity decay. Characteristic oscillatory patterns are observed, most clearly for the experiments in the gas mixture with 10 % O_2.

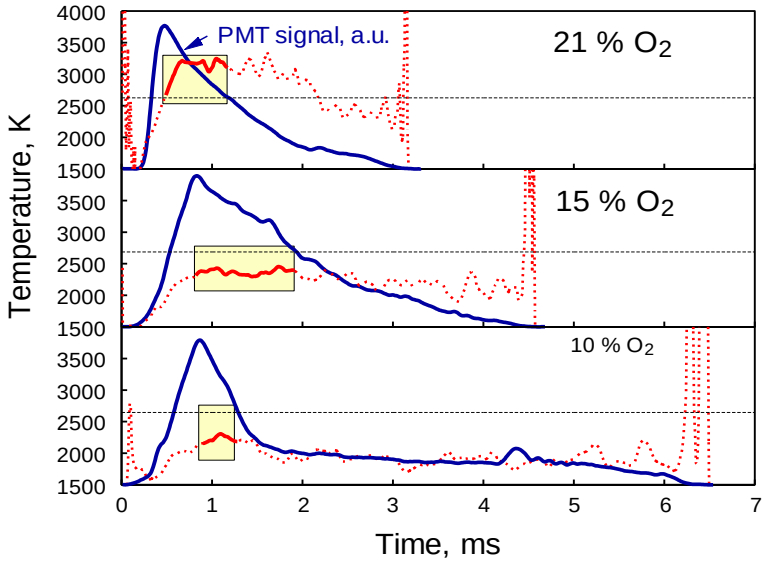

Figure 3.6 Emission traces measured through a 568 nm filter and temperature traces obtained from the emission intensity ratio measured at 589 and 532 nm. All results are for approximately 6 μm aluminum particles. See text for further details.

Strong temperature oscillations at the beginning and the end of each trace do not represent true temperatures and are caused by the reduced amplitude of the emission signals, so that their ratios vary dramatically. For all temperature traces, the temperature continues to increase even after the emission traces pass over their peak values. Following this initial increase, the temperature is stabilized and then slowly decreased at longer burn times for all particles. For the particle burning in air, the maximum instantaneous temperature is close to 3200 K. As the particle is burning out, its temperature drops to and remains at about 2400 K. For the particles burning at reduced oxygen concentrations, the temperatures are respectively lower. The changes in the temperature during the burn time are also less pronounced than in air.

For each particle, the highest characteristic combustion temperature was determined. This temperature was found as an average of the temperatures measured after the emission signal peaked and until the emission signal value was above one half of its peak amplitude. To illustrate this averaging routine, horizontal dashed lines in Figure 3.6 cross the emission traces at the levels corresponding to one half of their peak values. The portions of the temperature traces used to obtain the averaged values are shown bold and are further highlighted by shaded panels. The characteristic particle temperatures obtained as described above are plotted as a function of the particle size in Figure 3.7. These data represent experimental points shown as filled circles in Figure 3.5. Two different approaches were used to obtain curve fits for the characteristic flame temperatures. In one approach, the data were fitted by a straight line. These fits are shown as solid lines for each gas composition in Figure 3.7.

In another approach, it was assumed that the flame temperature is independent on the particle size for all particles burning in a diffusion-limited regime. Because this combustion regime is anticipated for large particles, the experimental data were described by a horizontal line for particles greater than some selected diameter, D_p*. This selected diameter represents the smallest particle diameter, for which a diffusion-limited combustion regime is observed. For particles smaller than D_p*, the data were described by another straight line, that had an adjustable slope representing an increase in flame temperature as a function of the particle size. Intercepts and slopes of both lines as well as the value of D_p*, corresponding to the horizontal coordinate of their cross-section point, were treated as adjustable parameters. These lines are shown as dotted lines in Figure 3.7.

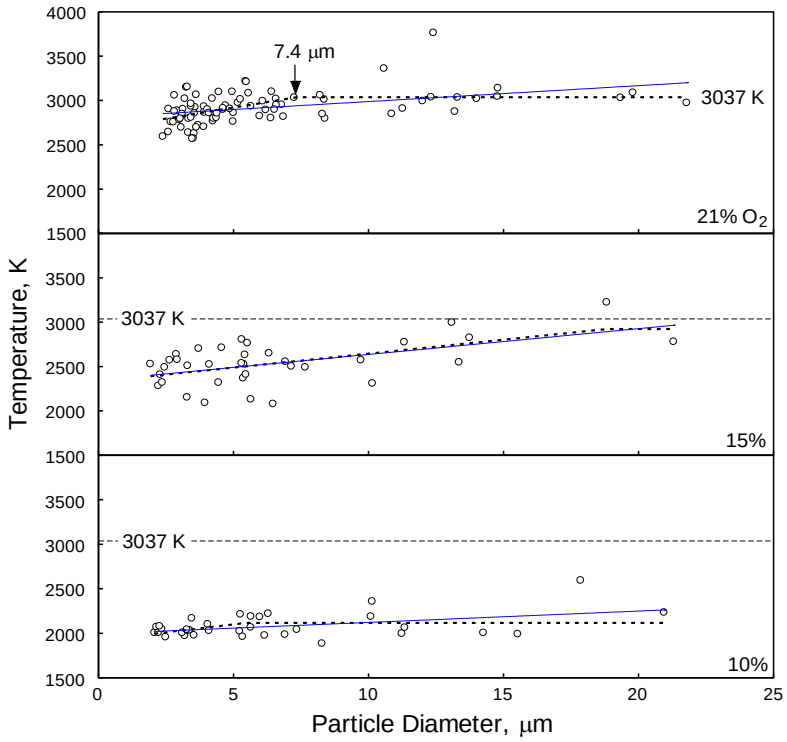

Figure 3.7 Average temperature distribution for Al in different atmospheres.

The goodness of fits was assessed using calculated sums of squared deviations shown in Table 3.2.

Table 3.2 Sums of Squared Deviations for One-line and Two-line Fits for the Temperature vs. Particle Size Data Shown in Figure 3.7

	Sum of squared deviations	
% O_2	***One line fit;***	***Two-line fit***
10	0.45	0.32
15	0.55	0.56
21	0.42	0.47

For particles burning in air, the straight line fit is overshooting the experimental points for large particle sizes. The two-line fit describes the data rather well (and better than the single line fit, as shown in Figure 3.7 and confirmed by calculated sums of squared deviations shown in Table 3.2). The sloped and horizontal lines cross each other at the particle size $D_p^* \approx 7.4$ μm. This implies that particles greater than this size burn in a gas diffusion-limited regime. For smaller aluminum particles, the temperature decreases indicating that the stand-off flame approaches the particle surface and surface reactions occurring at lower temperatures play an increasingly greater role in aluminum combustion. The steady temperature corresponding to the gas diffusion-limited combustion is 3037 K. This temperature level is also shown by dashed lines for the plots corresponding to the lower oxygen concentrations.

In agreement with the observations made for individual temperature traces shown in Figure 3.6, the averaged temperatures are substantially reduced for experiments at 15 and 10 % of O_2. For the case of 15 % O_2, the single line fit effectively coincides with the two-line fit. For the two-line fit, the sloped and horizontal lines are predicted to cross at $D_p^* \approx 19$ μm. Therefore, a slow increase in the combustion temperature occurs as a

function of the particle size practically for the entire range of particle sizes considered. The temperature almost reaches the 3037 K level as the particle size increases to 20 μm. Therefore, it can be concluded that in the O_2/N_2 mixtures with 15 % of O_2, diffusion-limited combustion regime is expected for particles greater than 20 μm.

For aluminum particles burning in the gas mixture with 10 % of O_2, the temperature is fairly constant for all particle sizes considered. It is relatively low, close to 1994 K, which is likely an indication of the surface-controlled combustion.

Finally, it is interesting to assess intensity of the molecular AlO emission produced by aluminum particles burning in different environments. AlO emission is a commonly used indicator of the vapor-phase combustion processes and is known to be prominent in the spectra produced by Al flames. A PMT signal filtered at 486 nm was used to track the AlO emission in this work. To provide a quantitative measure of the AlO emission intensity that can be applied to different particles and environments, the emission measured at 486 nm, was related to that measured at 568 nm (outside of the main AlO peaks). Further, to remove the effect of particle temperature on the tracked intensity ratio, it was divided by the ratio of the calculated emission intensities I_{486nm}/I_{568nm} for the black body emitter at the same temperature as the instant temperature of the burning particle. In a confirmatory experiment, this ratio, $\frac{\left(I_{486nm}/I_{568nm}\right)_{\exp}}{\left(I_{486nm}/I_{568nm}\right)_{bb}}$ was determined for a tungsten lamp and was found to be equal to one. Thus, when this ratio is greater than one, it would imply a non-negligible AlO emission.

Characteristic intensity ratios as a function of time for the particles burning in environments with 21 and 10% of O_2 are shown as dotted lines in Figure 3.8. Respective temperature traces are also shown for each particle.

For the particle burning in 21 % O_2, the AlO emission is very strong at short burn times. Interestingly, for the specific trace shown in Figure 3.8 as well as for all other examined traces, the AlO emission is peaking before the maximum in the combustion temperature is reached. When the temperature reaches its steady level just above 3000 K, the AlO emission is already reduced compared to its peak value and remains relatively steady. A noticeable decrease in the AlO emission begins somewhat before the decrease in the particle temperature. The characteristic correlation between temperature and AlO emission traces described above for particles burning in air are less noticeable for particles burning at lower oxygen concentrations, for which the changes in both temperature and AlO emission as a function of time are less pronounced. However, in all cases, the maximum AlO emission is attained prior to the peak temperature. It is also worth noting that, as shown in Figure 3.8, even at the lowest oxygen concentration, the $\frac{\left(I_{486nm}/I_{568nm}\right)_{\exp}}{\left(I_{486nm}/I_{568nm}\right)_{bb}}$ ratio is noticeably greater than 1, indicating a non-negligible presence of vapor-phase AlO.

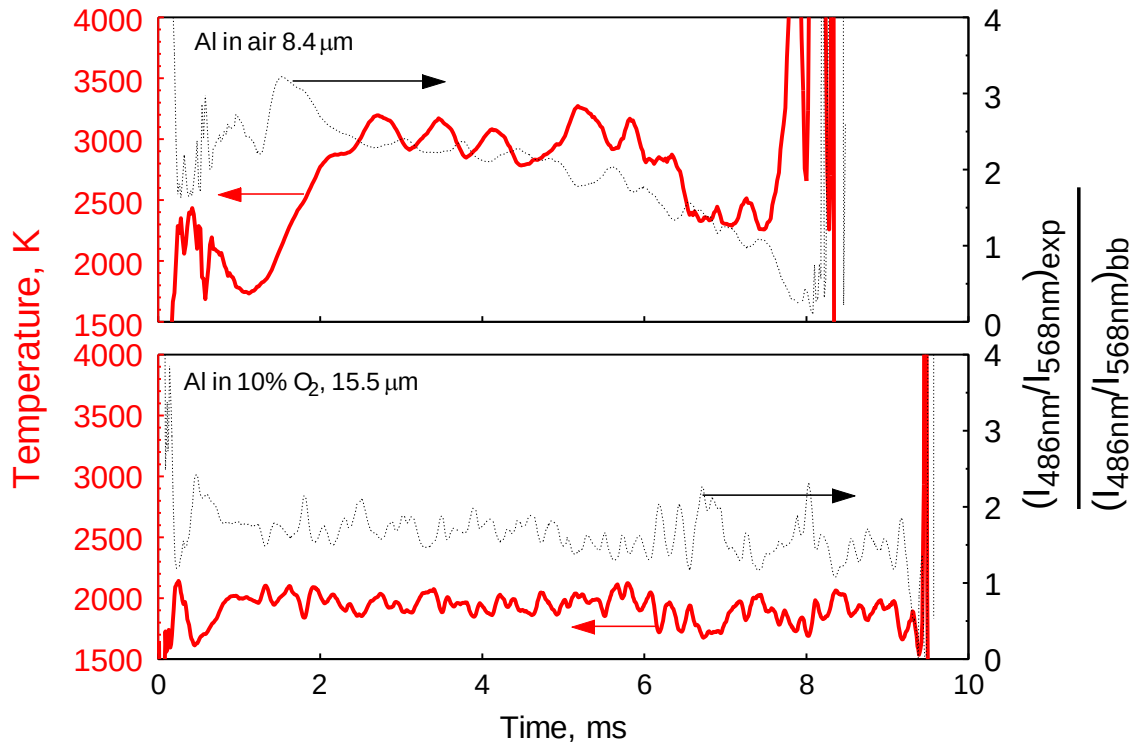

Figure 3.8 Traces showing particle temperatures (solid lines) and intensity ratios (dotted lines) characterizing the molecular emission of AlO for particles burning in different environments.

3.4 Discussion

It is interesting to interpret changes observed in the optical signatures of the micron-sized Al particles burning in air presented in Figures 3.6 and 3.8 in context of the reported earlier combustion scenario for large Al particles [13]. In reference [13], Al combustion in air was described to include three stages. In the first stage, the measured temperature was close to 3000 K; it decreased nearly stepwise to about 2750 K in the second stage. Finally, during the third stage, the temperature decreased to about 2200 K. The interpretation of that staged behavior proposed in refs. [13, 37] took into account possible dissolution of oxygen in the burning metal. Initially, formation of a saturated Al-O solution reduces the boiling point of Al and thus reduces the overall flame temperature

for particles burning with distinct vapor phase flame. Further, the homogeneous liquid solution separates into distinct liquid phases, so that the spherical symmetry of the particle and its flame is destroyed resulting in an oscillatory emission pattern. Sharp directional changes in particle trajectories shown in Figure 3.3 provide further evidence for the asymmetric burn. Finally, as the particle burns out, the flame approaches its surface and eventually reaction becomes controlled by the surface oxidation. The maximum temperature observed for combustion of micron-sized Al particles in air (cf. Figures 3.6, 3.8) is remarkably close to the flame temperature reported in reference [13] for the stage one combustion. In addition, current data for the early burn times show clearly how the particle temperature increases prior to reaching the maximum flame temperature. This temperature increase could not have been detected in reference [13] where particles were generated by a micro-arc discharge, so that their initial temperature was near the Al boiling point. The time during which the initial temperature increase is observed in this work, can be interpreted as the time required to establish a vapor-phase flame for a self-heating Al particle. This interpretation is further supported by the observed rapid increase and peak in the AlO emission occurring during this initial temperature ramp. Once the quasi-steady vapor phase flame is established, AlO emission becomes weaker, likely due to a more complete conversion of the evaporating Al into Al_2O_3. As the data suggest, the duration of this transient initial process is comparable to the duration of the initial, quasi-steady combustion stage, occurring at about 3000 K. As for larger particles, the initial combustion stage is followed by a substantial reduction in the flame temperature. This temperature decrease is likely explained by transition from a nearly spherically symmetric vapor phase flame to a mixed combustion regime, when

rates of heat release due to surface oxidation and reaction of the evaporated Al are comparable to each other. The reduced role of the vapor phase reaction is also supported by the reduced intensity of the AlO emission, as seen in Figure 3.8. Stages 2 and 3 described earlier for large Al particles are difficult to distinguish for micron-sized particles studied here, most likely due to their significantly weaker overall emission intensity.

The discussion above applies to particles greater than about 7 μm burning in air, for which the temperature traces follow the characteristic patterns shown in Figures 3.6 and 3.8. For finer particles burning in air, the maximum flame temperatures are lower, indicating that the full-fledged vapor phase flames were never achieved. This effect is most clearly seen in Figure 3.7. It is very consistent with the predictions of reference [38] where a maximum particle size is estimated, below which the vapor-phase flame alone cannot be self-sustaining because of the increased rate of heat losses to the cold surroundings. The critical size estimated in reference [38] for air is 6 μm, which correlates well with the particle size of 7.4 μm, for which the flame temperature reaches its maximum quasi-steady level as shown in Figure 3.7. Similarly, the vapor-phase flames are not produced in environments with reduced oxygen concentrations for any particles less than 20 μm considered in this work. However, even for particles burning at the lowest oxygen concentration, observations of both oscillatory emission patterns (Figure 3.6) and greater than one factor measuring the AlO emission intensity (Figure 3.8) suggest that the vapor phase reactions are not negligible. Unfortunately, this means that the reaction model describing Al particle combustion adequately cannot be readily reduced to either vapor phase or surface reaction models.

It is expected that a feasible and practically useful modeling approach can be developed if the combustion event is separated into several subsequent stages. For example, these stages can include a period while a vapor-phase flame is established, a quasi-steady, diffusion limited combustion, transition to the surface reaction, and quenching. For each stage, an expression for the burn rate can be proposed based on mechanistic understanding of the processes occurring in experiment. Data from the present experiments would serve to develop and/or validate such expressions. In particular, future models will benefit from detailed comparisons with individual particle combustion characteristics, such as overall emission times, temperature and black body and AlO emission intensity traces. Once validated, new dynamic models can replace current, steady-state models, e.g., described in reference [21], used to predict contribution of the metal combustion processes in complex reactive systems.

3.5 Conclusion

Combustion processes for micron-sized Al particles burning in air can be separated into several stages. Initially, a transient process is observed during which the measured flame temperature is increasing and molecular AlO emission peaks. It is interpreted as formation of a vapor-phase flame around a self-heating Al particle. This transient process is followed by a period when the flame temperature is stable around its maximum value just exceeding 3000 K while the AlO emission remains relatively strong. It is suggested that during this stage, the reaction is controlled by the vapor-phase combustion. In the following reaction stage, both the flame temperature and AlO emission are decreasing until the particle is extinguished. During this final stage, the vapor phase flame is

suggested to approach the particle surface, and the reaction continues with an increased contribution from surface oxidation.

The characteristic maximum flame temperatures for aluminum particles burning in air are slightly higher than 3000 K for particles greater than 7.4 μm; the temperatures are decreasing for finer particles. These observations are interpreted to suggest that particles less than 7.4 μm do not attain a full-fledged vapor phase flame, which is produced for coarser particles.

When oxygen concentration is reduced to 15 %, the maximum flame temperature of 3000 K is not attained even for the coarsest, 20 μm particles considered here. The temporal changes in the recorded particle emission signatures diminish, so that it is more difficult to distinguish between different stages in particle combustion. At 10 % oxygen concentration, combustion occurs at a nearly constant temperature close to 2000 K, indicating a surface-reaction controlled process. This temperature is not changing substantially for particles of different sizes. However, the AlO emission is substantial even for particles burning at about 2000 K, suggesting a non-negligible vapor phase reaction.

It is suggested that a useful description of the aluminum combustion dynamics must break the entire combustion process into several stages, so that different reaction mechanisms active at different burn times can be described separately. Descriptive reaction rates should be introduced for each stage, based on the experimental observations and understanding of the respective reaction mechanisms.

CHAPTER 4

EXPERIMENTAL ACCURACY ASSESSMENT

Results discussed in a previous chapter presented experimental trends characterizing combustion of aluminum particles. Experimental settings and parameters, such as the operating photomultiplier voltages, laser offset distance, gas flow rates, and CO_2 laser power were fixed between experiments. Generally, these parameters determine the sensitivity of the present measurements, e.g., the smallest particle size that can be worked with, the lowest flame temperature necessary for useful optical measurements, etc. Before proceeding to test on other systems, it is important to explore how significant the above restrictions and limitations were in affecting the trends characterizing aluminum particle combustion. This chapter presents and discusses experiments conducted with substantially altered experimental settings and the effects on the results.

4.1 Problem Statement

Analysis of aluminum burn durations shown in Figure 3.5 uses a conventional d^n law with an exponent n usually dependent on the reaction rate-limiting process. For a spherically symmetric, diffusion-limited combustion, n is close to 2, while for a kinetics-limited reaction the value of n is close to 1 [43]. Values between 1 and 2 are commonly expected for intermediate combustion regimes. However, in the present experiments, the value of n is substantially less than 1, which is somewhat unusual. The results show an apparently very weak effect of particle sizes on their burn time. Before attempting to interpret such results, it is suggested that additional validating experiments are necessary.

Another justification for additional experiments has come from data analysis [44] where the measured temperature traces for individual particles of known sizes were used to calculate the heat release from each particle taking into account convective heat transfer for a hot particle in air. Transition heat transfer model developed for situations when both free-molecular transport and continuum convection processes must be accounted for [38], was used in these calculations for μm-sized particles. In different calculations, the particle was either assumed to remain at the constant initial size or it was assumed to grow in size, accounting for the oxide formed based on the heat released by the particle. Results of these calculations suggested that for smaller particles, the amount of heat released based on the measured temperature traces may be greater than the total heat of oxidation for the starting particle. Thus, the accuracy of the particle size and temperature measurements was questioned and additional experiments were designed and performed.

4.2 Approach

Using the same experimental setup described in the previous chapters, additional experiments were designed for aluminum particle combustion in air. The first experimental issue addressed in these new tests was possible errors in the particle size measurements. It was noted that the minimum particle size resolved from the measurements of the amplitudes of the scattered light pulses was determined by the noise in the PMT output. The noise was tracked to the DC power supply used, which was replaced for these measurements with a battery. Reduced noise enabled us to increase the gain of the respective PMT, so that sensitivity of the system to fine particles was noticeably increased. Figure 4.1 shows a particle size distribution comparison of

commercially determined and experimental scattered-light measurements taken before and after the setup modification.

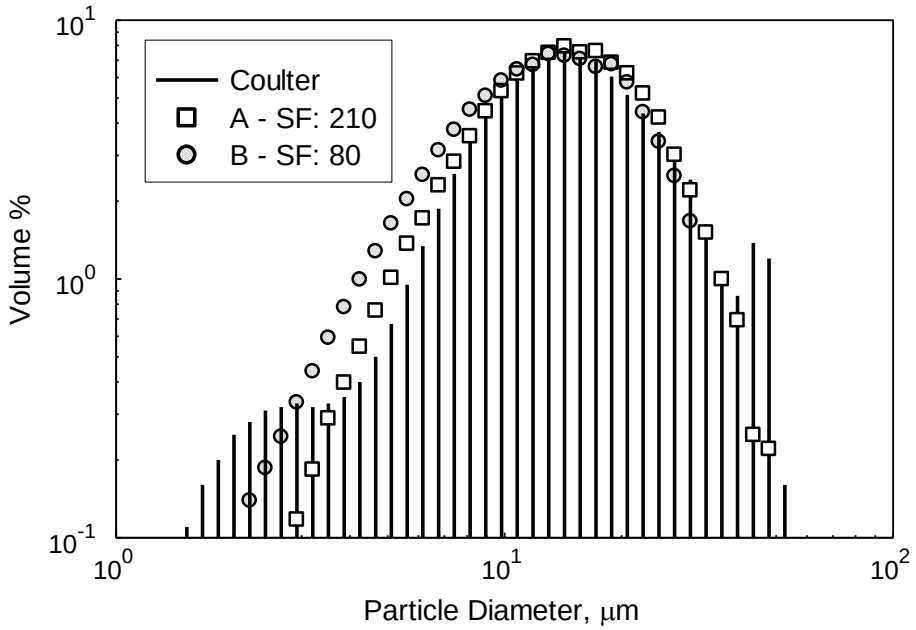

Figure 4.1 Particle size distribution comparison from a commercially determined device (Coulter) and two light scatter experiments.

Experiment A with a scaling factor (SF) of 210 shows the previously reported experiment in comparison to the amplified settings for the current Experiment B with a scaling factor of 80. The substantial differences in sensitivity between the two light scatter experiments were evident in the disparity of the scaling factor. Despite the differences, both measurements matched well to the particle size distribution obtained with a commercial device implying that measured scattered pulses for each experiment produced comparable particle size distributions in the 1-30 μm size range. Note that an increase in sensitivity for finer particles and a sharp drop in detection of particles greater than 30 μm is observed in Experiment B. This effect is caused by a limited dynamic range of the PMT. Despite minor differences, the two size distributions measured before

and after the modification were largely consistent between them and compared well with the Coulter-measured particle size distribution.

To improve the accuracy of temperature measurements for fine particles, the sensitivity of the respective PMT measuring filtered particle emission was increased. This, similar to the light-scattering measuring PMT, was achieved by an increased DC voltage from the PMT power supply. Furthermore, in addition to individual particle temperature measurements, spectra were taken during a test from emission of multiple particles; these spectra were processed to establish the implied emission temperature. The fiber optic of an irradiance calibrated spectrometer (StellarNet EPP2000) was positioned at the brightest combustion zone of burning particles. Due to low light emission from individual particles, spectra were captured using an extended integration time of the spectrometer (typically, 35 seconds). The approximate temperature from the representative spectrum was computed using Planck's law [45] with a prefactor to accommodate a grey body assumption for particles. This temperature was compared to that measured from the filtered PMT intensity ratio.

4.3 Results and Discussion

Upon matching the scatter and emission pulses, the following procedure was used to identify the particles, for which the measured emission times were representative of the burn durations, i.e, particles with the longest burn times, as described in [15]. Both particle size range and burn times were broken down into selected bins. For the previous experiment, four particle size bins of 2-6, 6-10, 10-14, and 14-20 μm were used. Due to a an improved detection limit and focus of the previous tests on smaller particles, the particle size bins for this experiment were 1.5-3, 3-5, 5-7, and 7-11 μm. Adjustment to

the bin sizes was necessary to maintain meaningful statistics. For each size bin, normalized cumulative distributions of the particle emission durations were obtained similar to Figure 3.4. The cutoff of 1.0 % was selected for both experiments instead of the previously reported 2.5 %.

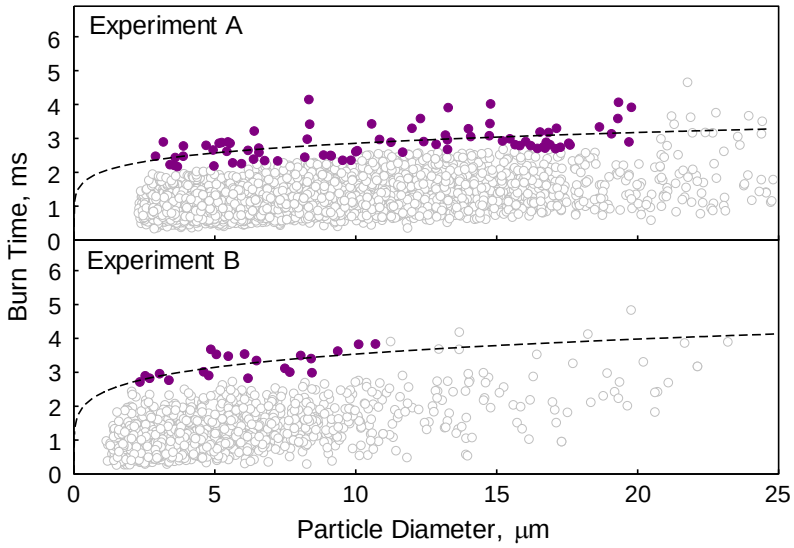

Figure 4.2 Burn times as a function of particle size for aluminum particles in air in both experiments.

Scatter plots for the previous experiment A and the current experiment B are shown in Figure 4.2. As discussed, the lower limit for particle detection from the previous experiment was observed at 2 μm while increased threshold detection was seen in experiment B with particles observed down to 1.5 μm. The particles above the 1.0 % cutoff criteria for each bin size range are shown by the filled symbols. Note that the processing presented in [14] did not properly reflect bin size selection discussed here. The selection algorithm had been adjusted in the processing and Figure 4.2 indicates the appropriate points for the current cutoff criteria. These points were further processed for particle combustion temperatures.

Burn time trends related to particle diameters were fitted using the $\tau_b = a \cdot D^n$ function that was previously used and indicated by the dashed line in Figure 4.2. The parameters *a* and *n* for each experiment in air for corrected points are shown in Table 4.1. The exponent values are 0.15 and 0.17 for experiments A and B, respectively. More scatter was evident in the previous data set compared to the current set as indicated by the correlation factor, *r*. Both experiments consistently indicated a weak experimental trend.

Table 4.1 Empirically-based Parameters for the $\tau_b = aD^n$ Fit for the Aluminum Particle Burn Times Measured in Air

	Experiment	*a*	*n*	Correlation, r^2
Aluminum	A	2.01	0.15	0.26
	B	2.40	0.17	0.46

Emission traces, such as one found for air in Figure 3.6, were analyzed for both runs and found to be qualitatively similar to each other and those presented earlier [15]. Features such as the initial peak, decay, and plateau of the signals were consistent. The corresponding temperatures connected to the three phases of combustion discussed in [14] were also similar for particles of the same size.

Selected particle temperatures for each experiment are shown as a function of particle size in Figure 4.3. These data represent experimental points shown as filled circles in Figure 4.2. Both experiments showed that average temperatures reach an upper limit of ~3100 K as particle size approaches 5 μm with similar conclusions drawn from the previous chapter with slightly different data. Though Experiment B lacked the quantity of data points found in the previous set, temperature trends at different particle sizes were shown to be within the same range as the previous data.

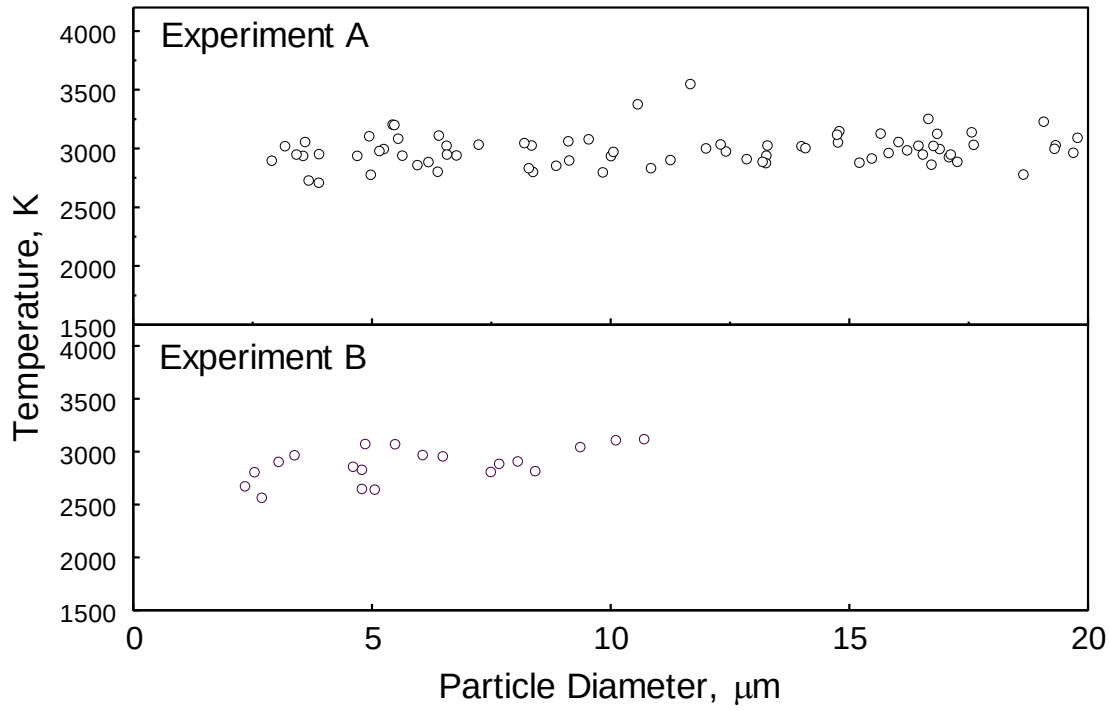

Figure 4.3 Average temperature distribution for both Al experiments in air.

A partial spectrum of multi-particle combustion shown in Figure 4.4 was analyzed for the implied temperature by fitting the Planck's law. This spectral region was exclusive of any molecular emission lines and best represents the assumed grey body emission. Inherent signal noise was due to low intensity levels. Since the spectrometer was allowed to integrate for the maximum duration, the spectrum contained individual particles burning as well as periods in which no emission instances were recorded. Furthermore, emission captured would be represented by the brightest burning particles since emission from those particles is most significant. The approximate temperature determined was 3026 K. This temperature was consistent to the upper-limit temperature observed in both previous and current experimental records.

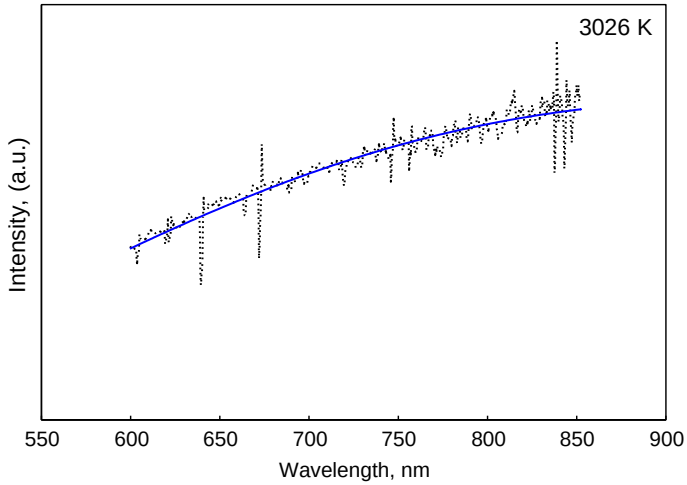

Figure 4.4 Multi-particle combustion spectrum fitted with a grey body adjusted Planck's law.

4.4 Summary

Combustion experiments in air were repeated and shown for comparison. In practical terms, the new experiment reproduced the previous data set within the error range of the system despite the substantial differences experimental settings. Size analysis produced similar trends in burn time as a function of particle diameter, and temperature observations were also consistent for both experiments. Captured emission spectrum confirmed the accuracy of the pyrometry. Overall, the repeatability of the experiments demonstrated that the apparatus and processing procedure used to analyze and interpret the results is repeatable.

CHAPTER 5

COMBUSTION DYNAMICS OF DIFFERENT REACTIVE MATERIALS

Experiments previously reported validated and determined the accuracy of the data for combustion of aluminum. It was of great interest to further expand the experimental data to other reactive systems that have not been studied or reported for the particle size range of interest. Materials presented in this chapter are aluminum-molybdenum oxide and aluminum-copper oxide thermites as well as other advanced materials such as aluminum-iodine and aluminum-boron-iodine. The experimental approach for studying these systems was identical to that used in studying aluminum particles. To accommodate the spark-sensitive nature of these materials, a vibratory feeder was utilized to entrain the particles in the gas stream.

5.1 Approach

Four advanced materials were prepared for analysis: $5.25Al{\cdot}MoO_3$, $8Al{\cdot}3CuO$, $Al{\cdot}I_2$ (20 wt. %), and $Al{\cdot}B{\cdot}I_2$. These particles were fed using a vibratory powder feeder shown schematically in Figure 5.1. A carrier gas flow was supplied to the tube. The powder loaded into the hopper does not fall through the opening until the entire assembly was vibrated using a speaker; the amplitude and frequency of the vibrations were adjusted to achieve a steady aerosol flow. The exit tube of the vibratory feeder was bent and inserted into an orifice to ensure one-dimensional vibration and particle flow along the vertical axis.

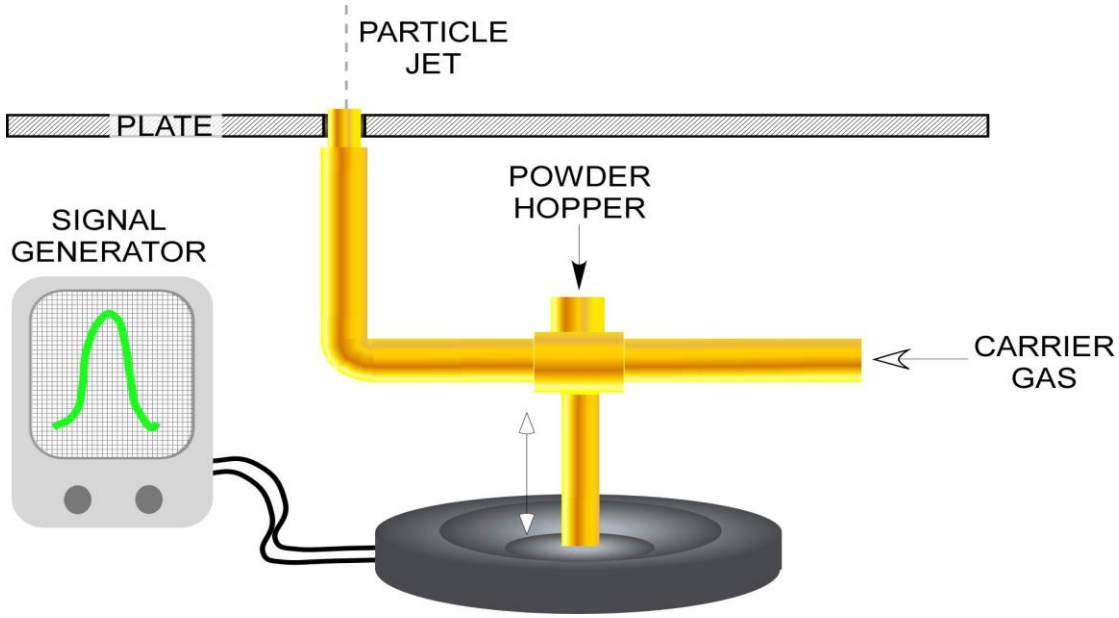

Figure 5.1 Illustration of vibratory feeder used to spark-sensitive reactive particles.

Diagnostics developed in the study of aluminum combustion was utilized for these experiments [14]. In the initial processing step, the powder particle size distribution measured by a commercial device Beckman-Coulter LS230 was compared to that implied from the amplitudes of the scattered 785 nm light pulses measured in this experiment. The scaling factor converting the scattered pulse amplitudes to the particle sizes was used as an adjustable parameter for each material.

Upon matching the scatter and emission pulses for each material, a bin selection procedure with a cutoff threshold [14], was used to represent the longest burning particles. A conventional d^n law normally used to describe burn time and particle size correlation [43] were fitted to the selected data meeting the cutoff threshold. These fitted lines were reported with the scatter plots of matched pulses.

Representative photographs of burning particle streaks were taken. Flow settings were selected so that for all materials the measured average particle velocities were close to 0.5 m/s.

Temperature was calculated using the ratio between signals measured from the filtered 589 nm and 532 nm photomultiplier tubes (PMT). The aluminum monoxide (AlO) molecular emission is a commonly used indicator of the vapor-phase combustion processes for Al flames. AlO emission was quantified from the ratio of intensities at 486 and 568 nm compared to the same intensity ratio for a black body emitter at the experimental particle temperature, $\frac{\left(I_{486nm}/I_{568nm}\right)_{\exp}}{\left(I_{486nm}/I_{568nm}\right)_{bb}}$, as discussed in more detail in reference [14].

The final processing step involved analysis of the emission, temperature, and AlO emission profiles for each material. Initially, observed temperature and AlO ratio oscillations at the beginning and the end of each trace due to very weak emission signals were discarded. Representative traces for ~5 μm diameter particle for all materials were reported. Subsets of the matched data dictated by cutoff criteria for each material were further analyzed. Average temperatures and AlO emission ratios were compared for particles of different sizes and for different stages of combustion. Selection of these signal portions was limited to emission peak value (100%) to the half of its peak value within each signal trace. Further analysis was done between 1 and 10 % of maximum emission level for a given trace if any evidence of a lower intensity burn at altered temperatures was found. It was noted that this analysis can be adjusted to accommodate other observations in the emission signals.

All combustion experiments were performed in air. Further discussion of experimental parameters and results for each material is presented in subsequent sections.

5.2 Aluminum-Molybdenum Oxide

A 50.4 wt. % MoO_3 and 49.6 wt. % Al elemental powder mixture was first prepared using the arrested reactive milling (ARM) [7]. The resulting powder composite was approximately $5.25Al{\cdot}MoO_3$ in composition. A scanning electron microscope (SEM) image of the material is presented on Figure 5.2. The material exhibited a rock-like morphology with sharp edges. Coarse particles were observed to be around 20 μm in length.

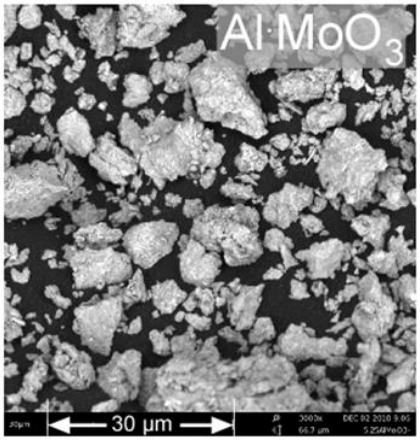

Figure 5.2 Scanning electron microscope (SEM) image of prepared $5.25Al{\cdot}MoO_3$ powder.

A comparison of particle size distribution from light scattering experiments and the Coulter LS230 commercial device is shown in Figure 5.3. Both distributions matched well for particles ranging from 1-20 μm in diameter. Overall, the match was imperfect in comparison to aluminum most likely due to the irregular morphology. However, the

salient features of the powder distributions in the finer fractions were represented well.

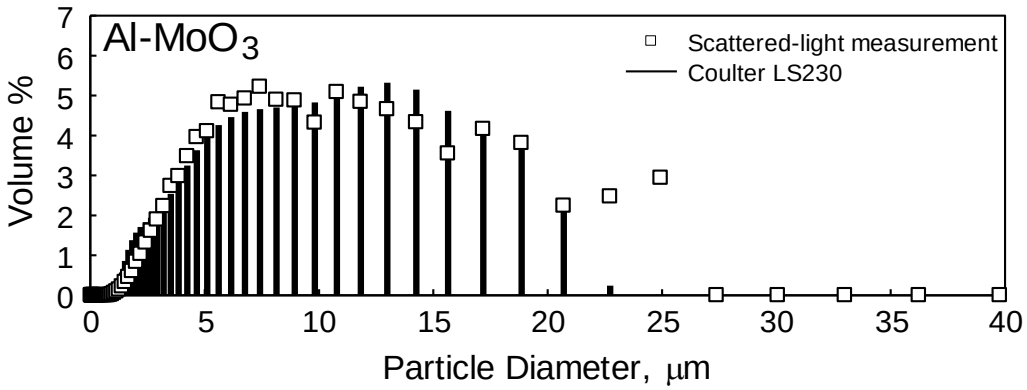

Figure 5.3 Particle size distribution of $Al{\cdot}MoO_3$ particles measured from a commercial device (Coulter LS230) and light scattering experiments.

Figure 5.4 shows the burning particle streaks of $Al{\cdot}MoO_3$. Multiple short streaks were observed; these streaks were likely produced by particles that were heated but not ignited or heated and partially burnt in the laser beam and were discounted from the data processing. Longest streaks found were likely to represent particles ignited when exiting from the CO_2 laser beam. These particles were included into the present analysis.

It was observed that streaks for $Al{\cdot}MoO_3$ particles exhibited changes in direction immediately after ignition; however, the following portions of the streaks were relatively straight. All $Al{\cdot}MoO_3$ particle streaks ended with characteristic spear points, produced when an emission decay is followed by its intensification.

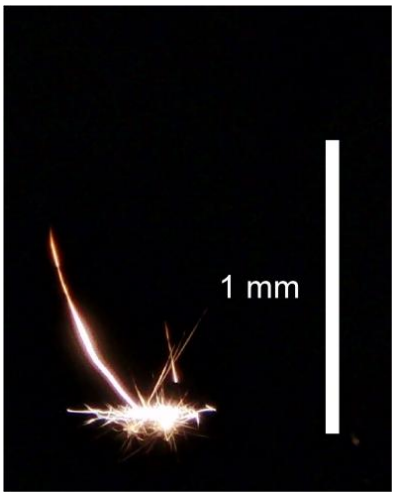

Figure 5.4 Photograph of burning particle streaks for 5.25Al·MoO_3.

Figure 5.5 shows a representative emission trace, temperature profile, and AlO ratios for a 5 μm Al·MoO_3 particle. Burn time for each particle trace was defined from the start the emission pulse above the noise level until the signal diminishes to the noise level. The observed burn duration for this particle was 6.8 ms which was much longer than the ~2.5 ms for aluminum of a similar particle size. It was also observed that the emission trace consisted of two parts. Initially, emission was relatively strong and the measured temperature peaked at about 2800 K. The emission then decayed to very low values but remained consistently above the noise. During that second reaction period, the temperature remained close to 2100 K. The AlO emission decayed at longer burn times and the overall level of AlO emission was substantially lower than for pure Al.

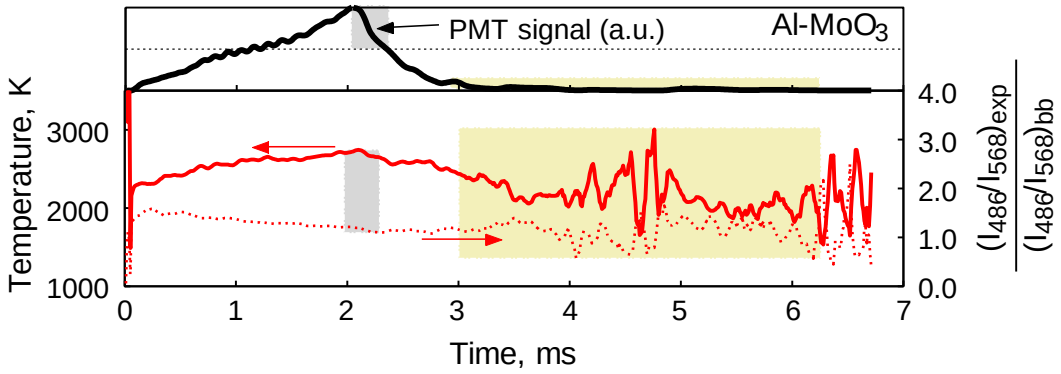

Figure 5.5 Emission and temperature trace for Al·MoO_3 burning in air.

Four particle size bins of 0.5-1.5, 1.5-2.5, 2.5-4, and 4-8 μm were used. The cutoff of was selected to be 3.0 % for the Al·MoO_3 particles.

Scatter plot shown in Figure 5.6 present the emission times as a function of the particle size for the matching pairs of emission and scattered light pulses for Al·MoO_3. Filled symbols show the subset of all data points above the 3.0 % cutoff of burn time in each respective bin size. In using the D^n relationship, the exponent n value of 0.18 was obtained for Al·MoO_3.

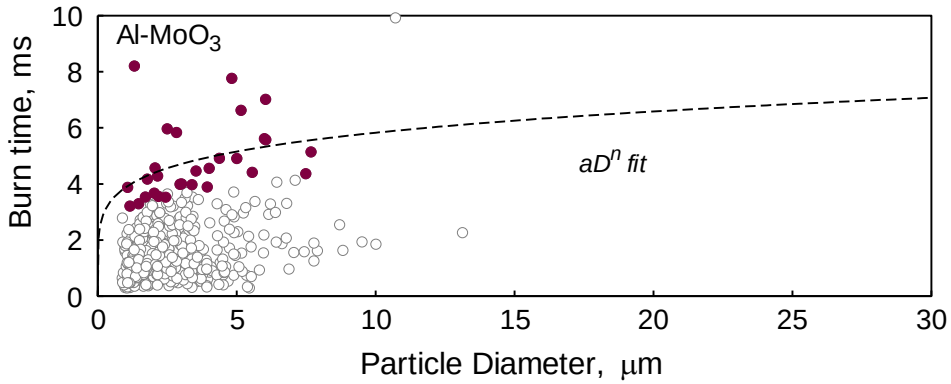

Figure 5.6 Burn time as a function of particle size for Al·MoO_3 burning in air.

A summary of the reported average temperature and AlO ratio is shown in Figure 5.7 for the regions within the signal traces represented by the shaded boxes in Figure 5.5.

Filled points represented the processing done using 50-100 % of PMT max while unfilled points were for processing using 1-10 % of the PMT peak value. The combustion temperature was observed to consistently decrease from ~2800 K to ~2100 K for all particle sizes when emission intensity decreases. The AlO emission remained relatively stable and weak for all particle sizes.

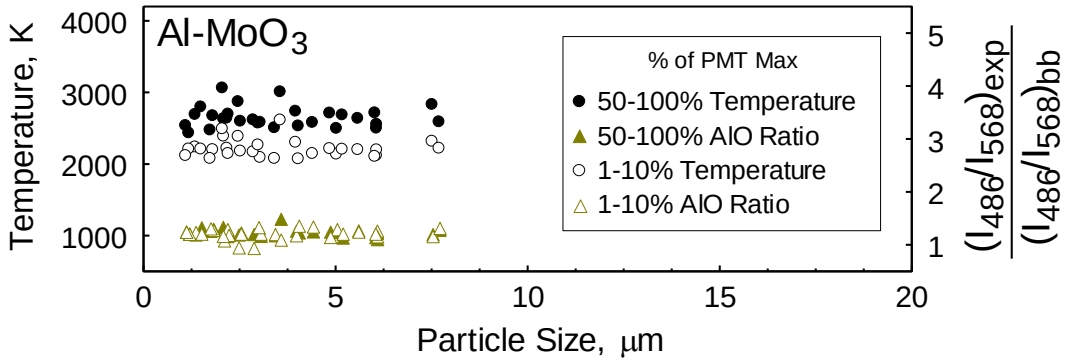

Figure 5.7 Average temperature and AlO ratio as a function of particle size for Al·MoO_3 burning in air.

5.3 Aluminum-Copper Oxide

Elemental powder mixture of aluminum and copper oxide discussed in detail in reference [7] for 8Al·3CuO was prepared using arrested reactive milling. The referenced paper described the irregular surface morphology as well as the internal complex of the material. The material also exhibited a coarse particle size greater than 100 μm in diameter.

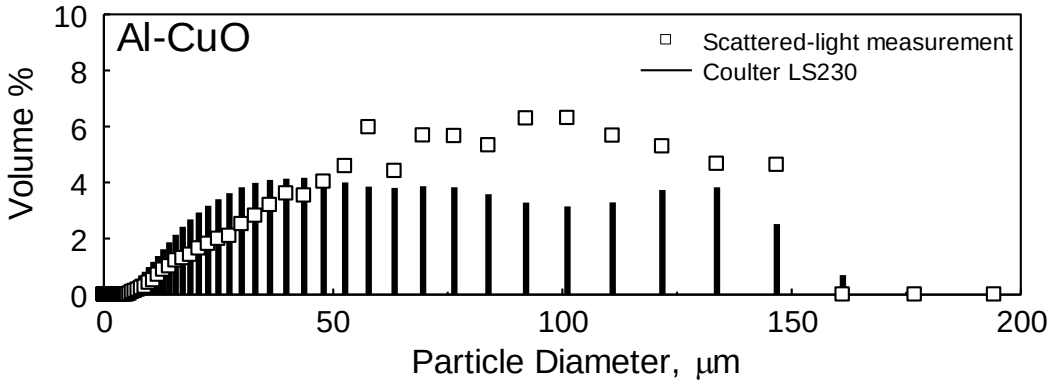

Figure 5.8 Particle size distribution of Al·CuO particles measured from a commercial device (Coulter LS230) and light scattering experiments.

A comparison of particle size distribution from light scattering experiments and the Coulter LS230 device is shown in Figure 5.8. Similarly to Al·MoO_3, the match between the distributions were imperfect in comparison to aluminum but the main features of the powder distributions were reasonable. It was worth noting that entraining coarse Al·CuO particles up to 150 μm as reported by the light scatter experiments was feasible by using the vibratory feeder.

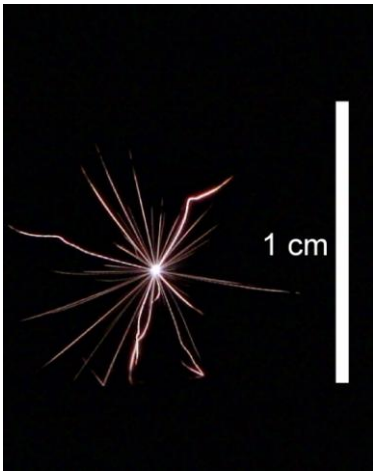

Figure 5.9 Photograph of burning particle streaks for 8Al·3CuO.

Burning particle streaks of Al·CuO particles is shown in Figure 5.9. It was observed that these particles exploded immediately after ignition with streaks being ejected in all directions. Some particle streaks maintained a straight path while other streaks continued to burn with sharp trajectory changes indicating a vapor phase flame prior to quenching. Audible micro explosions were reported which no other tested material exhibited. This phenomenon was mainly due to the expected evaporation of the reduced Cu. This occurs because the adiabatic reaction temperature for Al·CuO thermite, 2823 K (calculated using CEA package [46]) is limited by the Cu boiling point,

Emission trace of a representative particle for Al·CuO shown in Figure 5.10 exhibited a strong emission peak which were found consistent with the experimental observations. This initial peak occurred earlier in comparison to aluminum and offered insight into the highly reactive nature of this material. As the particle emission gradually decays, the observed temperature remains steady prior to quenching while the AlO ratio remains steady. The burn duration for this particle was 3 ms which was practically comparable to that of aluminum of equivalent size. Similar to Al·MoO_3, it was also observed that the emission trace consisted of two parts: emission peak with prior to a temperature at 2600 K followed by continuous decay of emission occurring at a temperature around 2500 K.

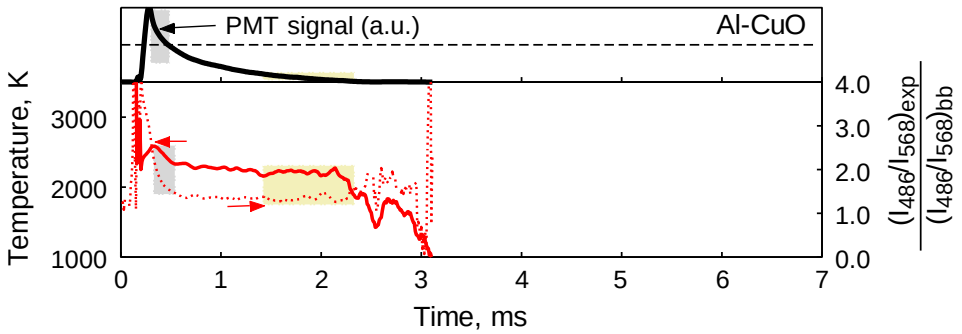

Figure 5.10 Emission and temperature trace for Al·CuO burning in air.

The four particle size bins used in this experiment were 5-10, 10-15, 15-25, and 25-50 μm were used. The cutoff of was selected to be 5.0 %.

Scatter plot for burn time of Al·CuO is shown in Figure 5.11. The d-power law fit yielded an exponent *n* value of 0.16 for Al·CuO.

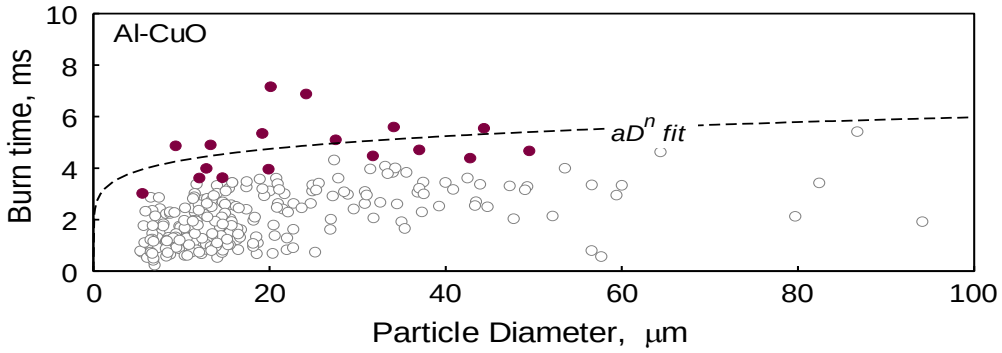

Figure 5.11 Burn time as a function of particle size for Al·CuO burning in air.

Reported average temperature and AlO ratio is shown in Figure 5.12. Combustion temperature was observed to consistently decrease from ~2400 K to ~2100 K throughout the size range. The observed temperatures were lower than for aluminum and were expected due to reduced enthalpies of combustion for the aluminum reaction due to the presence of other species. The average AlO emission was observed to decrease throughout all reported particles. This difference observed for average AlO emission, however, is most likely an artifact of the noise in the analyzed 50-100% peak value region (as shown in the shaded area on the left in Figure 5.10) compared to the 1-10% region.

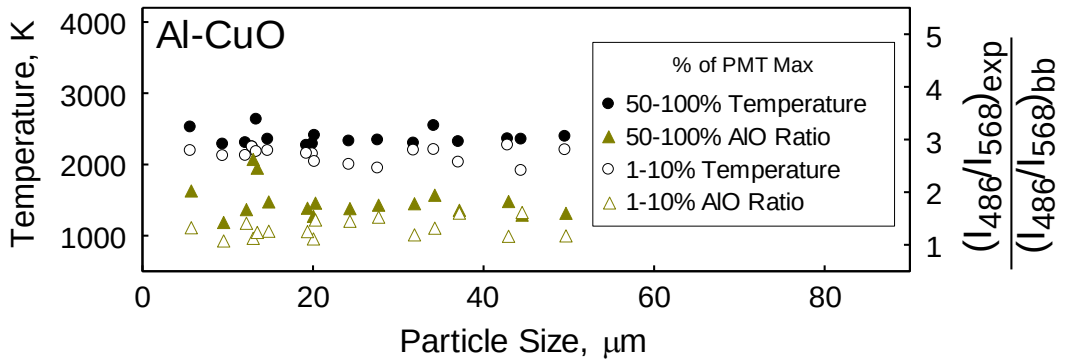

Figure 5.12 Average temperature and AlO ratio as a function of particle size for Al·CuO burning in air.

5.4 Aluminum-Iodine

Aluminum-iodine materials were recently developed for the purpose of bio-agent defeat applications [47]. Preparation of these materials was done through cryogenic milling so that volatilization of iodine was minimized [48]. The material selected for combustion experiments was $Al \cdot I_2$ (20 wt % I_2). A scanning electron microscope (SEM) image of the material is presented on Figure 5.13. The material exhibited a rock-like morphology similar $Al \cdot MoO_3$. Images also indicated that a significant amount of fine particles ranging from 5 μm and smaller were present.

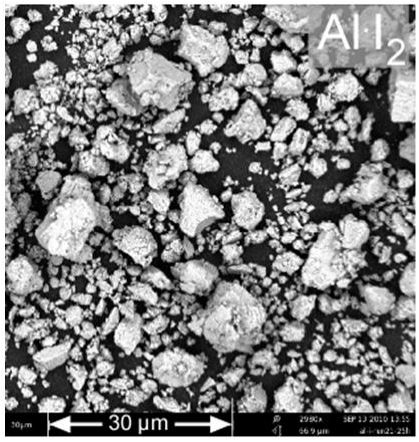

Figure 5.13 Scanning electron microscope (SEM) image of prepared Al·I_2 (20 wt % I_2) powder.

Particle size distribution comparison between experimental light scattered measurements and the commercial device is shown in Figure 5.14. Discrepancies in matching the finer fraction of the powder were observed when the particle distribution as reported by the commercial device ranged from sub-micron to coarse diameters of 36 µm. Similar to previously reported powders, the match between the distributions of particle diameters was imperfect in comparison to aluminum but the main features of the powder distributions were reasonable to 27 µm in diameter.

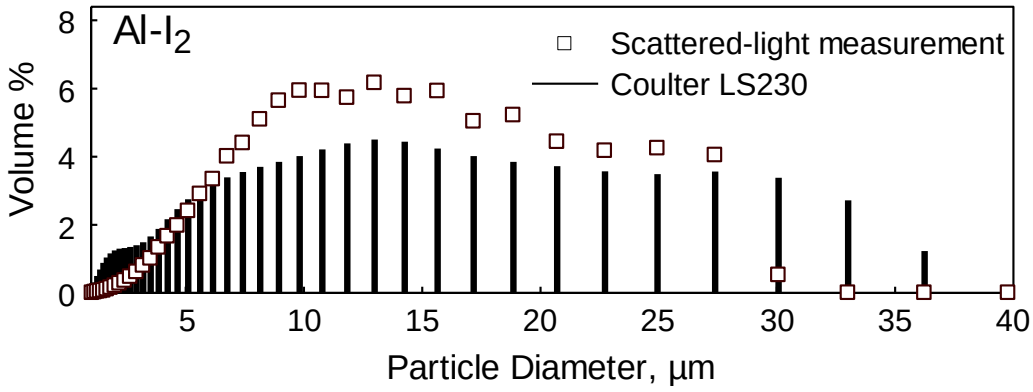

Figure 5.14 Particle size distribution of Al·I_2 particles measured from a commercial device (Coulter LS230) and light scattering experiments.

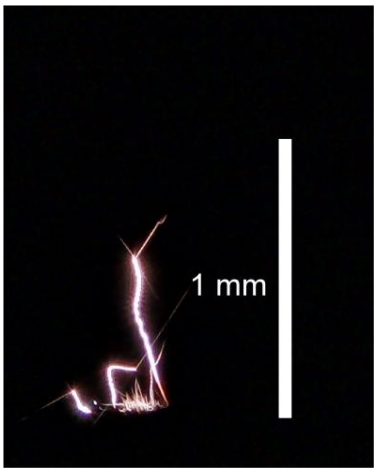

Figure 5.15 Photograph of burning particle streaks for $Al \cdot I_2$.

Streaks produced by $Al \cdot I_2$ particles shown in Figure 5.15 indicated both sharp changes in the particle direction and distinct oscillations. These phenomena are characteristics of an asymmetric vapor phase flame. Characteristic micro-explosion patterns are repeatedly observed by the end of the streaks.

Emission trace of a representative particle for $Al \cdot I_2$ shown in Figure 5.16 began with pronounced oscillations. The burn duration of 5.5 ms was found to be longer than aluminum and the discussed thermite systems of similar size. The emission intensity increased and reached its peak value after a long burn time. However, the temperature of the burning particle increased rapidly and remained nearly steady, at about 2600 K for the entire combustion event. The intensity of AlO emission was less than for pure Al.

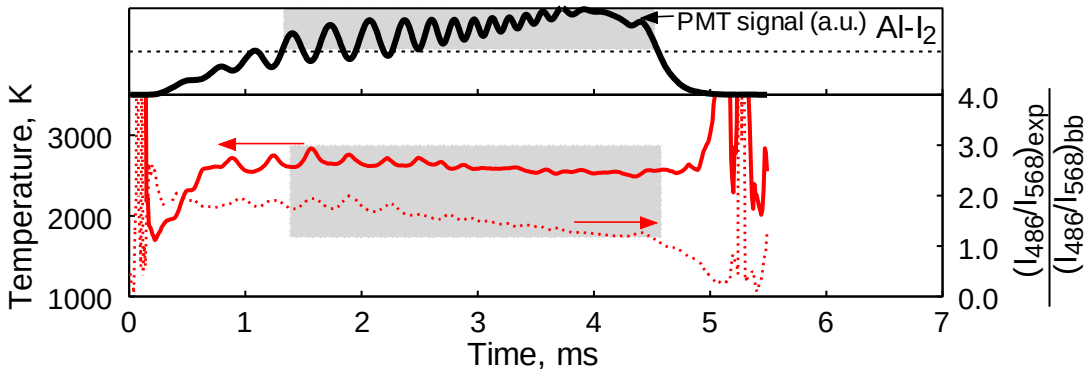

Figure 5.16 Emission and temperature trace for Al·I_2 burning in air.

The four particle size bins used in this experiment were 0.5-1.5, 1.5-3, 3-5, and 5-8 µm were used. The cutoff of was selected to be 1.0 %.

Scatter plot for burn time of Al·I_2 is shown in Figure 5.17. The d-power law fit yielded an exponent *n* value of 0.01.

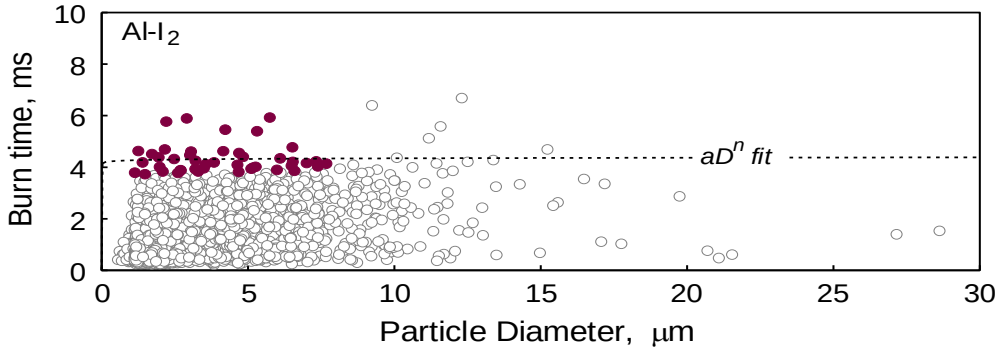

Figure 5.17 Burn time as a function of particle size for Al·I_2 burning in air.

For Al·I_2, average values of temperature and AlO emission is obtained when the emission trace was between 50 and 100 % of its maximum value and shown in Figure 5.18. Both average AlO emission level and temperature remained remarkably stable for all particles with the values consistent to those observed in the individual trace shown in Fig. 5.16.

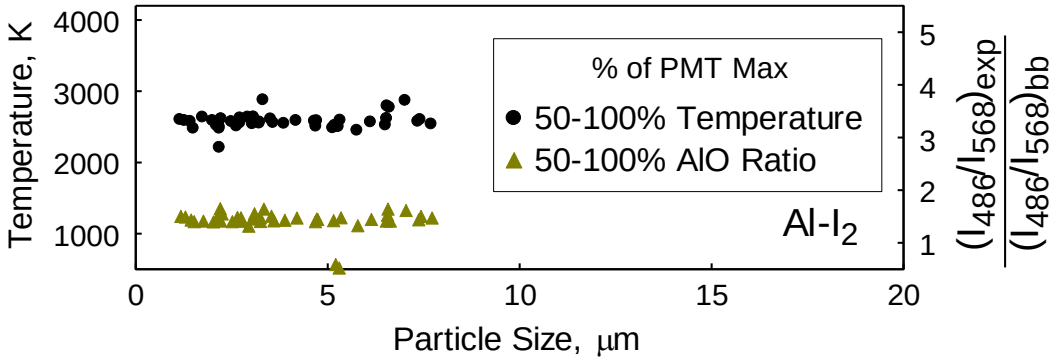

Figure 5.18 Average temperature and AlO ratio as a function of particle size for Al·I_2 burning in air.

5.5 Aluminum-Boron-Iodine

Boron reaction systems have been of primary interest by virtue of having the highest energetic density (per unit mass) in comparison to aluminum and other materials [49]. However, the main problem in developing boron-based materials was the difficulty of ignition due to high boiling point of the boron. In an effort to enhance the combustion characteristics of boron while utilizing its energetic density, an aluminum-boron-iodine material was developed. Elemental powders (11 wt. % B, 20 wt. % I_2, and 69 wt. % Al) of each component were mechanically milled in a shaker mill [50]. The surface morphology of the material, as shown in the SEM image found in Figure 5.19, exhibited a rock-like morphology similar other milled materials. Unlike the other materials, the surface of the particles featured rounder edges.

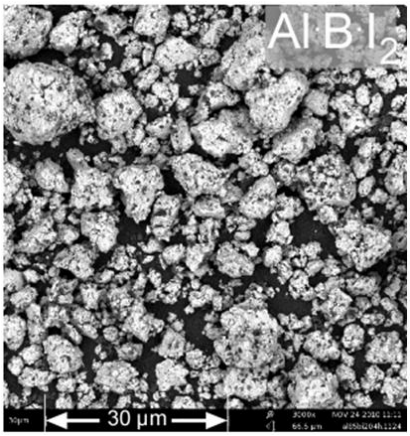

Figure 5.19 Scanning electron microscope (SEM) image of prepared Al·B·I_2 (11 wt. % B, 20 wt. % I_2, and 69 wt. % Al) powder.

The wide range of the particles sizes seen in the SEM image is also evident in the particle size distribution shown in Figure 5.20. Similar to Al·I_2, the match between the distributions of particle diameters was imperfect in comparison to aluminum but the salient features of the powder distributions were represented well.

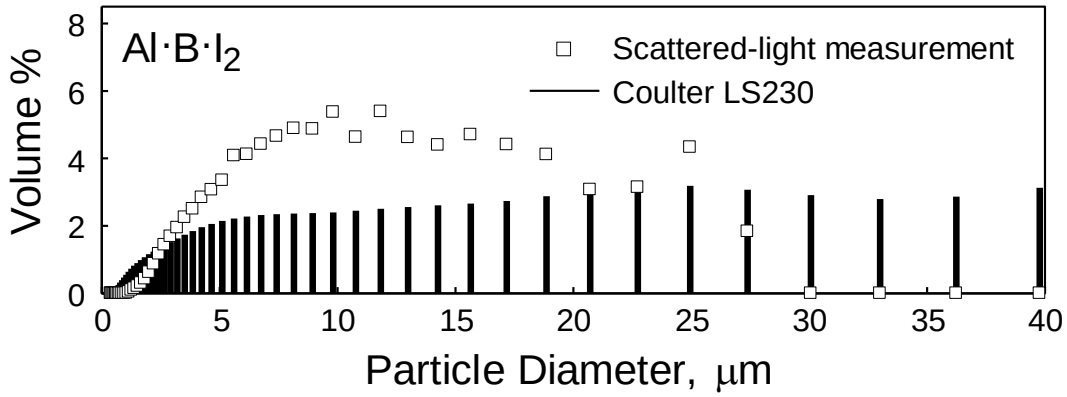

Figure 5.20 Particle size distribution of Al·B·I_2 particles measured from a commercial device (Coulter LS230) and light scattering experiments.

An image of burning streaks for Al·B·I_2 particles is presented in Figure 5.21. One of the captured particle streaks exhibited the longest burning streak in comparison to other materials presented indicating a more sustained combustion reaction. Thin streaks

observed and the sharp changes in trajectory suggested a predominant surface reaction and asymmetric burning flame with gas ejections.

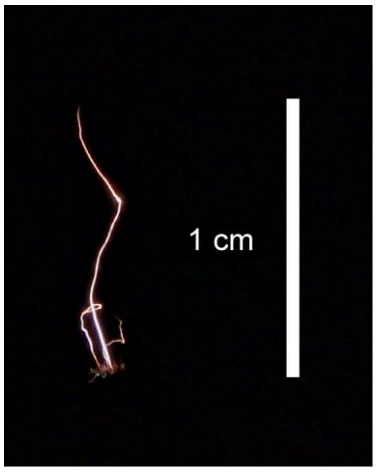

Figure 5.21 Photograph of burning particle streaks for Al·B·I_2.

Emission trace of a representative particle for Al·B·I_2 shown in Figure 5.22 had a burn duration of 10 ms which was longer than any previously discussed traces. Emission peak and temperature peak were concurrent with both traces gradually extinction as time progressed. Temperature of the burning particle reached as high as 3100 K which was comparable to peak temperatures found in aluminum.

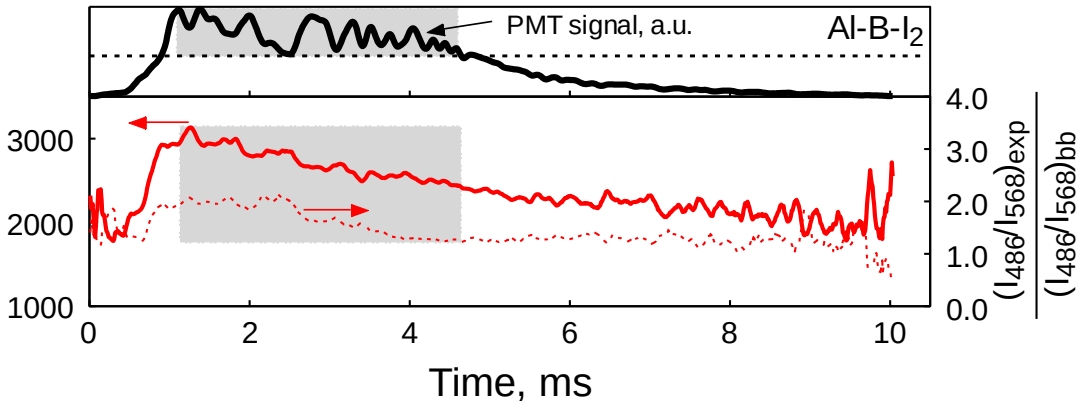

Figure 5.22 Emission and temperature trace for Al·B·I_2 burning in air.

The four particle size bins used in this experiment were 0.9-2.2, 2.2-3, 3-4, and 4-8 µm were used. The cutoff of was selected to be 3.0 %.

Scatter plot for burn time of Al·B·I_2 is shown in Figure 5.23. The d-power law fit yielded an exponent *n* value of 0.13.

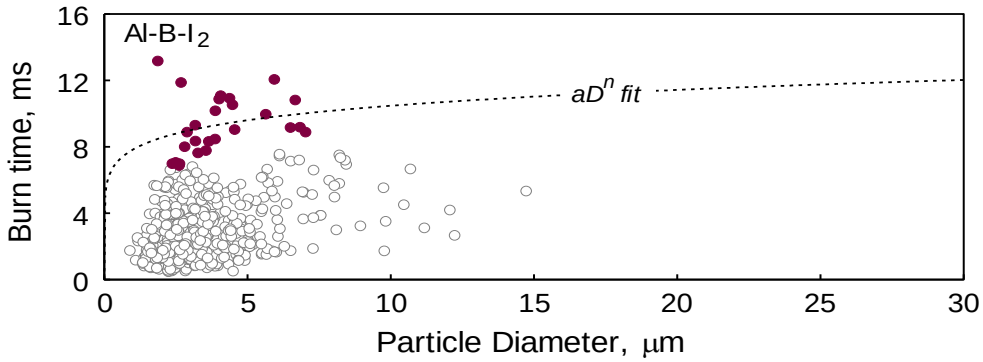

Figure 5.23 Burn time as a function of particle size for Al·B·I_2 burning in air.

For Al·B·I_2, average values of temperature and AlO emission shown in Figure 5.24 is obtained when the emission trace was between 50 and 100 % of its maximum value similar to Al·I_2. Average values of temperature and AlO ratio had a wide scatter in comparison to previous materials. Higher temperatures up to 3800 K were reported for these particles; however a known atomic emission line of boron around the 589 nm wavelength interfered with temperature measurement. It was proposed that further experiments measuring temperature for this system required different wavelength spectrum.

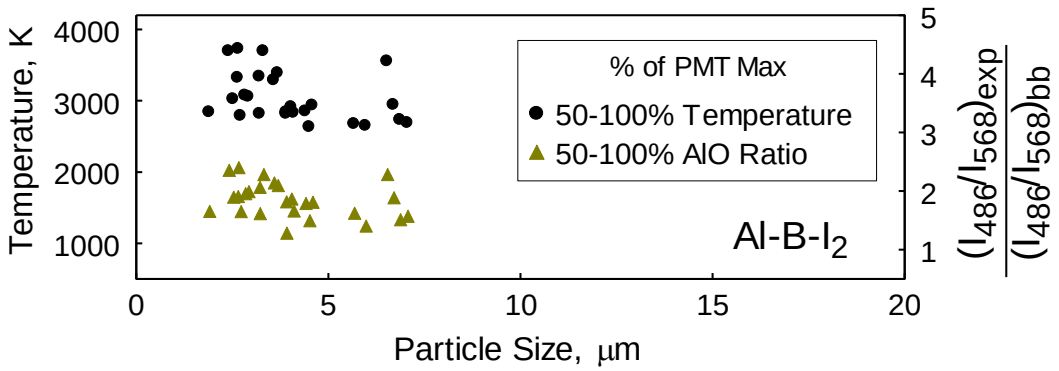

Figure 5.24 Average temperature and AlO ratio as a function of particle size for $Al \cdot B \cdot I_2$ burning in air.

5.6 Summary

Energetic systems of $Al \cdot MoO_3$, $Al \cdot CuO$, $Al \cdot I_2$, and $Al \cdot B \cdot I_2$ have been characterized through a variety of methods. Light scattering experiments provided comparable fits matching salient features of the particle size distribution for these materials despite the morphological features. Multiple short streaks were observed in all systems. Burning streaks as well as individual emission traces for 5μm particle were in agreement and indicated that $Al \cdot B \cdot I_2$ burned the longest in relation to other materials tested. Comparison of burn times for the complete range of particles suggested a weak correlation with respect to particle diameter, which is consistent with other reported empirical data [6]. This conclusion suggests that burn time analysis using the *d-power* law is not adequate. Furthermore, the weak particle size dependency suggests that combustion for these advanced materials is mainly limited by either diffusion or kinetics of the reaction system – further experimental work is necessary.

CHAPTER 6

CONCLUSION

The present work established an approach for measuring and characterizing combustion parameters of fine, 2-20 μm reactive powders of metal-based materials. The experiments reported here are focused on the aluminum-based compositions. For pure aluminum, particle combustion is characterized for different oxidizers, including oxygen, carbon dioxide, and water. Particle combustion times are obtained from the optical emission of burning particles. The present results are compared with the literature data for burn time trends as a function of particle size, which were derived based on earlier experiments for coarser aluminum powders. The comparisons show that the previously reported trends are not valid for the finer powders addressed in this study. The measured burn times are significantly longer than implied by the proposed earlier correlations and exhibit a very weak dependence on the particle size. Optical signatures of individual micron-sized aluminum particles burning in different environments show characteristic oscillatory patterns previously observed for much larger particles. Such optical signatures highlight the importance of the heterogeneous processes in aluminum combustion. For aluminum burning in water vapor, the optical signature of the particle is substantially weaker than in other environments, indicating a primarily surface oxidation.

Subsequent work expanded the experimental setup to include optical sensors for pyrometry and tracking molecular AlO emission. The data processing was further refined for better reproducibility, and the analysis for aluminum combustion in oxygenated atmospheres was revisited. Combustion regimes for vapor-phase and surface-reaction as

well as transition heat and mass transfer regimes found for fine particles combusting in air are discussed. The experimental results further suggested that the complete descriptions for the reaction mechanism should be inclusive of multiple burning stages occurring at different characteristic temperature ranges, which were also observed in previous papers.

Because of the surprisingly weak effect of particle size on the measured burn times, a critical analysis of the experimental setup was conducted. Results that were reported previously were validated after substantial modification of the setup and its settings. Validation measurements addressed the powder particle sizes, burn time trends, and temperature measurements. Pyrometric temperature readings for aluminum combustion were verified by the temperatures obtained from time-integrated spectra recorded using a calibrated spectrometer.

Combustion characterization were obtained for powders of nanocomposite materials prepared by arrested reactive milling, including the compositions of $Al \cdot MoO_3$, $Al \cdot CuO$, $Al \cdot I_2$, and $Al \cdot B \cdot I_2$. Burning characteristics such as the emission signatures, burn times, and temperatures were reported for all the materials. For all composite powders, the burn times were found to be longer and the combustion temperatures lower compared to the pure aluminum particles. A weak dependence of burn time on particle size suggesting inadequacy for using the d^n *(d-power-n)* law to describe the combustion time for such fine particles was also observed for these materials systems. Further work is necessary to elucidate the mechanistic reaction details.

Experimental limitations of the present approach are discussed including discrepancies in the interpretation of particle sizes for non-spherical powders measured in

situ in the present experimental setup vs. those measured by a commercial instrument, as well as limitations of the temperature measurements by the present optical pyrometer.

This work summarizes experimental efforts on single particle combustion for various aluminum-based reactive materials. Results in terms of the particle burn times, temperatures, and characteristic AlO emission as a function of the particle size reported for these materials will serve to guide the development of respective combustion models. Such models are of significant interest, especially for aluminum used as a fuel additive in a wide range of energetic formulations. Further research can apply the experimental methodology developed here to characterize combustion for variety of other reactive materials of interest, including pure metals, alloys, and composite powders.

REFERENCES

1. Price, E. W. "Combustion of Metalized Propellants," *Progress in Astronautics and Aeronautics* Vol. 90, 1984, pp. 479-513.

2. Shafirovich, E., and Varma, A. "Metal-CO_2 propulsion for Mars missions: Current status and opportunities," *Journal of Propulsion and Power* Vol. 24, No. 3, 2008, pp. 385-394.

3. Yetter, R. A., Risha, G. A., and Son, S. F. "Metal particle combustion and nanotechnology," *Proceedings of the Combustion Institute*. Vol. 32, 2008, pp. 1819-1838.

4. Dreizin, E. L. "Metal-based reactive nanomaterials," *Progress in Energy and Combustion Science* Vol. 35, No. 2, 2009, pp. 141-167.

5. Bockmon, B. S., Pantoya, M. L., Son, S. F., Asay, B. W., and Mang, J. T. "Combustion velocities and propagation mechanisms of metastable interstitial composites," *Journal of Applied Physics* Vol. 98, No. 6, 2005, pp. 1-7.

6. Lynch, P., Krier, H., and Glumac, N. "A correlation for burn time of aluminum particles in the transition regime," *Proceedings of the Combustion Institute* Vol. 32, 2009, pp. 1887-1893.

7. Stamatis, D., Jiang, Z., Hoffmann, V. K., Schoenitz, M., and Dreizin, E. L. "Fully dense, aluminum-rich Al-CuO nanocomposite powders for energetic formulations," *Combustion Science and Technology* Vol. 181, No. 1, 2009, pp. 97-116.

8. Farley, C., and Pantoya, M. "Reaction kinetics of nanometric aluminum and iodine pentoxide," *Journal of Thermal Analysis and Calorimetry* Vol. 102, No. 2, 2010, pp. 609-613.

9. Johnson, C. E., Higa, K. T., and Albro, W. R. "Nanothermites with condensable gas products. ," *Proceedings of the 35th International Pyrotechnics Seminar* Vol. 35, 2008, pp. 159-168.

10. Martirosyan, K. S., Wang, L., and Luss, D. "Novel nanoenergetic system based on iodine pentoxide," *Chemical Physics Letters* Vol. 483, No. 1-3, 2009, pp. 107-110.

11. Washburn, E. B., Trivedi, J. N., Catoire, L., and Beckstead, M. W. "The simulation of the combustion of micrometer-sized aluminum particles with steam," *Combustion Science and Technology* Vol. 180, No. 8, 2008, pp. 1502-1517.

12. Washburn, E. B., Webb, J. A., and Beckstead, M. W. "The simulation of the combustion of micrometer-sized aluminum particles with oxygen and carbon dioxide," *Combustion and Flame* Vol. 157, No. 3, 2010, pp. 540-545.

13. Dreizin, E. L. "Experimental study of stages in aluminum particle combustion in air," *Combustion and Flame* Vol. 105, No. 4, 1996, pp. 541-556.

14. Badiola, C., Gill, R. J., and Dreizin, E. L. "Combustion characteristics of micron-sized aluminum particles in oxygenated environments," *Combustion and Flame* Vol. 158, No. 10, 2011, pp. 2064-2070.

15. Gill, R. J., Badiola, C., and Dreizin, E. L. "Combustion times and emission profiles of micron-sized aluminum particles burning in different environments," *Combustion and Flame* Vol. 157, No. 11, 2010, pp. 2015-2023.

16. Gill, R. J., Mohan, S., and Dreizin, E. L. "Sizing and burn time measurements of micron-sized metal powders," *Review of Scientific Instruments* Vol. 80, No. 6, 2009.

17. Price, E. W., and Sigman, R. K. "Combustion of aluminzed solid propellants," *Progress in Astronautics and Aeronautics* Vol. 185, 2000, pp. 663-687.

18. Palaszewski, B., Ianovski, L. S., and Carrick, P. "Propellant technologies: Far-reaching benefits for aeronautical and space-vehicle propulsion," *Journal of Propulsion and Power* Vol. 14, No. 5, 1998, pp. 641-648.

19. Woodward Waesche, R. H. "Mechanisms and methods of suppression of combustion instability by metallic additives," *Journal of Propulsion and Power* Vol. 15, No. 6, 1999, pp. 919-922.

20. Zhang, F., Murray, S., and Gerrard, K. "Aluminum Particles-air Detonation at Elevated Pressures," *Shock Waves* Vol. 15, No. 5, 2006, pp. 313-324.

21. Beckstead, M. W. "Correlating aluminum burning times," *Combustion, Explosion and Shock Waves* Vol. 41, No. 5, 2005, pp. 533-546.

22. Shoshin, Y. L., and Dreizin, E. L. "Particle combustion rates for mechanically alloyed Al-Ti and aluminum powders burning in air," *Combustion and Flame* Vol. 145, No. 4, 2006, pp. 714-722.

23. Huang, Y., Risha, G. A., Yang, V., and Yetter, R. A. "Effect of particle size on combustion of aluminum particle dust in air," *Combustion and Flame* Vol. 156, No. 1, 2009, pp. 5-13.

24. Bucher, P., Yetter, R. A., Dryer, F. L., Vicenzi, E. P., Parr, T. P., and Hanson-Parr, D. M. "Condensed-phase species distributions about Al particles reacting in various oxidizers," *Combustion and Flame* Vol. 117, No. 1-2, 1999, pp. 351-361.

25. Marion, M., Chauveau, C., and Gökalp, I. "Studies on the ignition and burning of levitated aluminum particles," *Combustion Science and Technology* Vol. 115, No. 4-6, 1996, pp. 369-390.

26. Olsen, S. E., and Beckstead, M. W. "Burn time measurements of single aluminum particles in steam and CO_2 mixtures," *Journal of Propulsion and Power* Vol. 12, No. 4, 1996, pp. 662-671.

27. Dreizin, E. L. "On the mechanism of asymmetric aluminum particle combustion," *Combustion and Flame* Vol. 117, No. 4, 1999, pp. 841-850.

28. Edward L, D. "Experimental study of aluminum particle flame evolution in normal and micro-gravity," *Combustion and Flame* Vol. 116, No. 3, 1999, pp. 323-333.

29. Huang, Y., Risha, G. A., Yang, V., and Yetter, R. A. "Combustion of bimodal nano/micron-sized aluminum particle dust in air," *Proceedings of the Combustion Institute* Vol. 31, No. 2, 2007, pp. 2001-2009.

30. Poletaev, N. I., and Florko, A. V. "Spectral studies of the gas component of an aluminum dust flame," *Combustion, Explosion and Shock Waves* Vol. 44, No. 4, 2008, pp. 437-443.

31. Goroshin, S., Kolbe, M., and Lee, J. H. S. "Flame speed in a binary suspension of solid fuel particles," *Proceedings of the Combustion Institute* Vol. 28, No. 2, 2000, pp. 2811-2817.

32. Goroshin, S., Mamen, J., Higgins, A., Bazyn, T., Glumac, N., and Krier, H. "Emission spectroscopy of flame fronts in aluminum suspensions," *Proceedings of the Combustion Institute* Vol. 31, No. 2, 2007, pp. 2011-2019.

33. Shoshin, Y., and Dreizin, E. "Particle combustion rates in premixed flames of polydisperse metal - Air aerosols," *Combustion and Flame* Vol. 133, No. 3, 2003, pp. 275-287.

34. Rossi, S., Dreizin, E. L., and Law, C. K. "Combustion of aluminum particles in carbon dioxide," *Combustion Science and Technology* Vol. 164, No. 1-6, 2001, pp. 209-237.

35. Servaites, J., Krier, H., Melcher, J. C., and Burton, R. L. "Ignition and combustion of aluminum particles in shocked $H_2O/O_2/Ar$ and $CO_2/O_2/Ar$ mixtures," *Combustion and Flame* Vol. 125, No. 1-2, 2001, pp. 1040-1054.

36. Mohan, S., Furet, L., and Dreizin, E. L. "Aluminum particle ignition in different oxidizing environments," *Combustion and Flame* Vol. 157, No. 7, 2010, pp. 1356-1363.

37. Dreizin, E. L. "Phase changes in metal combustion," *Progress in Energy and Combustion Science* Vol. 26, No. 1, 2000, pp. 57-78.

38. Mohan, S., Trunov, M. A., and Dreizin, E. L. "On possibility of vapor-phase combustion for fine aluminum particles," *Combustion and Flame* Vol. 156, No. 11, 2009, pp. 2213-2216.

39. Glassman, I., and Yetter, R. A. *Combustion*. Burlington, MA: Academic Press, 2008.

40. Bazyn, T., Krier, H., and Glumac, N. "Oxidizer and pressure effects on the combustion of 10-μm aluminum particles," *Journal of Propulsion and Power* Vol. 21, No. 4, 2005, pp. 577-582.

41. Bazyn, T., Krier, H., and Glumac, N. "Evidence for the transition from the diffusion-limit in aluminum particle combustion," *Proceedings of the Combustion Institute*. Vol. 31, 2007, pp. 2021-2028.

42. Lynch, P., Krier, H., and Glumac, N. "Emissivity of aluminum-oxide particle clouds: Application to pyrometry of explosive fireballs," *Journal of Thermophysics and Heat Transfer* Vol. 24, No. 2, 2010, pp. 301-308.

43. Glassman, I. *Combustion*. San Diego, CA: Academic Press, 1987.

44. Wang, B., Badiola, C., Mohan, S., and Dreizin, E. L. "Combustion Dynamics of Aluminum Particles in Air," *AIChE Annual Meeting* Minneapolis, MN, 2011.

45. Holman, J. P. *Heat Transfer*. New York, NY: McGraw Hill, 2009.

46. Gordon, S., and McBride, B. J. "Computer Program for Calculation of Complex Chemical Equilibrium Compositions and Applications," *NASA Reference Publication 1311*, 1996.

47. Zhang, S., Schoenitz, M., and Dreizin, E. L. "Mechanically alloyed Al-I composite materials," *Journal of Physics and Chemistry of Solids* Vol. 71, No. 9, 2010, pp. 1213-1220.

48. Badiola, C., Schoenitz, M., Zhu, X., and Dreizin, E. L. "Nanocomposite thermite powders prepared by cryomilling," *Journal of Alloys and Compounds* Vol. 488, No. 1, 2009, pp. 386-391.

49. Yeh, C. L., and Kuo, K. K. "Ignition and combustion of boron particles," *Progress in Energy and Combustion Science* Vol. 22, No. 6, 1996, pp. 511-541.

50. Aly, Y., Schoenitz, M., and Dreizin, E. L. "Aluminum-Based Ternary Reactive Composite Powders," *AIChE Annual Meeting*. Minneapolis, MN, 2011.